Precision Measurements in Atomic Hydrogen

N. Kolachevsky[1,2], J. Alnis[1], A. Matveev[1,2], Th. Udem[1], R. Holzwarth[1,3], and T. W. Hänsch[1,4]
[1] *Max–Planck–Institut für Quantenoptik, Hans–Kopfermann–Str. 1, 85748 Garching, Germany*
[2] *P.N. Lebedev Physics Institute, Leninsky prosp. 53, 119991 Moscow, Russia*
[3] *MenloSystems GmbH, Am Klopferspitz 19, 82152 Martinsried, Germany*
[4] *Ludwig–Maximilians–University, Munich, Germany*

(Dated: July 24, 2007)

I. INTRODUCTION

Being the simplest of all stable atoms, the hydrogen atom is a crucial test object for a number of different fundamental theories. Its atomic properties can be calculated with unprecedented accuracy. At the same time, the level structure can be accurately probed using spectroscopy methods in the visible, near-IR and near-UV spectral regions. Almost a century ago, such tests gave birth to quantum physics clearly underlining the importance of high-resolution spectroscopy methods [1]. Today, the hydrogen atom plays an important role in determining fundamental constants and atomic parameters. During the last decade spectroscopic experiments on hydrogen and deuterium atoms have yielded new accurate values for the Rydberg constant [2], the ground-state Lamb shift [3], the deuteron structure radius [4], and the $2S$ hyperfine structure [5, 6]. Measurements of the Lamb shift and the $2S$ hyperfine structure permit sensitive tests of quantum electrodynamics (QED), which are based on comparisons between experimental values and results from corresponding QED calculations (for review see [7, 8]). Moreover, combining optical frequency measurements in hydrogen with results from other atomic systems, stringent upper limits for a possible slow variation of the fine-structure constant have been derived [9].

The employment of frequency combs turned high-precision optical frequency measurements into a routine procedure, readily available for a broad scientific community [10, 11]. The unprecedented accuracy of the frequency comb combined with the development of new ionic, atomic and molecular optical frequency references have opened wide perspectives for optical atomic clock applications in metrology, navigation and fundamental physics.

Continuous progress in optical frequency standards allows not only for more accurate tests of established theories, but also opens the possibility for new sensitive tests, that touch a broad variety of fundamental problems. Quantum electrodynamics which describes electromagnetic interactions on a quantum level, has not yet encountered discrepancies with experimental results. The theory of electro-weak interactions treats electromagnetic and weak interactions as two aspects of a unified interaction. The strong interactions can be adequately described within the theory of quantum chromodynamics. All of them operate with the fixed number of parameters (fundamental constants) which cannot be calculated within these theories. It is believed that at very high energies these theories can be unified in form of a grand unified theory (GUT). In this case the coupling constants will merge into a unified coupling constant α_{GUT} (see e.g. [13]). The theories of electromagnetic, weak and strong interactions are all based on Einstein's equivalence principle which does not allow a spatial or temporal variation of the coupling constants.

On the other hand, attempts to unify electromagnetic, weak and strong interactions with gravity encounters severe difficulties. To build such a "theory of everything" it seems that one has to extend the number of dimensions of our usual time-space world. For example, the Kaluza-Klein theory operates in the five-dimensional world, while string theories use up to 11 dimensions. The believe is that additional dimensions are compactified, so that the universe extends in these extra dimensions for only about the Planck length $L_{\mathrm{PL}} = \sqrt{G\hbar/c^3} \approx 1.5 \times 10^{-35}\,\mathrm{m}$, which is many orders of magnitude smaller then any other known physical length.

String theories may allow for temporal and spatial variation of the coupling constants that could be associated with cosmic dynamics. Some possible mechanisms that lead drift or spatial variations of the fundamental constants are discussed in literature [14–17]. As of now it seems that there is no sufficient theoretical evidence to make any well-grounded prediction of the size of such variations. For this reason experimental search is the appropriate way to look for new physics beyond the standard model. Among the variety of different methods, laboratory frequency measurements have become competitive very recently in terms of sensitivity to a possible variation of the fine structure constant in the present epoch. Though the time interval covered by these measurements is restricted to a few years, very high accuracy compensates for this disadvantage such that their sensitivity becomes comparable with astrophysical and geological methods operating on a billion-year time scale.

In this Chapter we give a description of the hydrogen beam experiment and methods of laser stabilization. Then, we will present the main principles of optical frequency measurements by the frequency comb technique using as an example the hydrogen $1S-2S$ line. The derivation of the Rydberg constant, the Lamb shift, measurements of the $2S$

hyperfine structure, and a brief discussion of corresponding QED tests will be given in the next section. In the last part we will show how the results of optical frequency measurements can be used to derive upper limits of the drift of fundamental constants. A comparison with results from sensitive non-laboratory measurements are presented.

II. TWO-PHOTON SPECTROSCOPY OF THE $1S-2S$ TRANSITION IN ATOMIC HYDROGEN

In the absence of external fields, the $2S$ level in atomic hydrogen decays to the ground $1S$ state via two-photon emission with the time constant of about 1/7 second. Taking into account that the $1S$ and the $2S$ levels are separated by 2.466×10^{15} Hz, the Q-factor of the $1S-2S$ transition is about 2×10^{15}. For many decades this value attracted close attention of spectroscopists, and a number of new methods to decrease the observed spectral line width have been invented. This dipole forbidden transition can be probed by means of Doppler-free two-photon spectroscopy with counter-propagating laser beams of equal frequencies. The required wavelength of $\lambda = 243$ nm can be generated either by a frequency doubled dye laser at 486 nm, or by quadrupling the frequency of titanium:sapphire or semiconductor laser at 972 nm. First experiments on two-photon spectroscopy of the $1S-2S$ transition started back in 1975, where a sample in a glass cells has been excited by a frequency doubled pulsed dye laser [18]. Since then, the experimental setup has been significantly improved: the cell has been replaced by an atomic beam apparatus. Remarkable progress has been made with the laser setup and the detection system. The improvements allowed to achieve a spectral resolution of 5×10^{12} which is still far away from the Q-factor defined by the natural line width. The current limit is due to contributions of velocity-dependent effects like time-of-flight broadening and the 2nd order Doppler effect [19]. Reducing the temperature of the hydrogen beam could solve these problems. The group of D. Kleppner at MIT [20] has shown experimentally that atomic hydrogen can be stored in magnetic trap and even Bose condensed, which significantly increases interrogation time and virtually eliminates contribution of the Doppler effect. However, collisional shifts of the $1S-2S$ line prevent precise spectroscopy in this case. On the other hand, trapping and cooling of atomic hydrogen in magneto-optical traps still appears to be difficult because of the specific level structure (excitation from the $1S$ state is always accompanied with ionization [21]) and technical difficulties to produce intense resonant light at 121 nm [22]. One possible route has been pointed out recently by D. Kielpinsky who proposes to use two photon laser cooling with the $1S-2S$ resonance by pulsed 243 nm light from a mode locked laser [23].

The resolution and accuracy of hydrogen $1S-2S$ measurements strongly depend on excitation and detection methods as well as on the stability of the interrogating laser. In the next Section we will describe the hydrogen spectrometer in Garching, starting with the description of the laser system used to excite the two-photon transition.

A. Laser system

For excitation of the $1S-2S$ transition in atomic hydrogen we use highly stable laser systems that deliver light at $\lambda = 243$ nm. In this section we present a dye laser operating on Coumarin 102 at 486 nm and a diode laser system at 972 nm designed for that purpose. While the former has been routinely used for high-precision measurements (see [9] for instance), the latter is planned to be transportable to use it for a variety of measurements in hydrogen-like exotic systems [24]. Comparing the requirements of our laser source to other stable laser sources used in metrological laboratories all over the world, there are two issues that require special attention. First, for efficient excitation of the $1S-2S$ transition one needs considerable power. This is because the two-photon transition is weak and Rabi frequencies on the order of 1 kHz are required because of the brief interrogation time available in an atomic beam. Secondly, the laser output is multiply transformed in non-linear processes (one doubling stage and two-photon transition for the dye laser and one additional doubling stage for the diode laser system). This fact imposes stringent requirements on the phase noise of the laser and on its spectral line shape [25].

For frequency stabilization of the dye laser we use a high-finesse cavity oriented with its axis horizontal that is located inside a temperature-stabilized vacuum chamber as shown in Fig. 1. The cavity is made from Ultra Low Expansion (ULE) glass and has a finesse of 90 000. We use a two-stage temperature stabilization system for suppressing thermal fluctuations of the cavity. The outer shell consists of an aluminum box with a layer of heat foils glued to all its sides. A 6-channel temperature controller maintains the temperature for each side within 100 μK (at the position of the corresponding sensor) by a fast two-point digital relay circuit. The internal stage is a conventional slow integrating circuit which heats the vacuum chamber to 31 °C. The residual temperature fluctuation on the surface of the vacuum chamber does not exceed 1 mK with a typical time constant of a few hours.

The frequency stabilization of the dye laser is made by means of the Pound-Drever-Hall phase modulation technique [26]. The optical locking scheme is very similar to the one presented in Fig. 2 (right). High servo loop bandwidth of about 3 MHz is reached using an intra-cavity electro-optical modulator (EOM). Measurements performed in 2003 have shown, that the typical short-term frequency drift does not exceed 0.5 Hz/s at 486 nm, while the spectral line

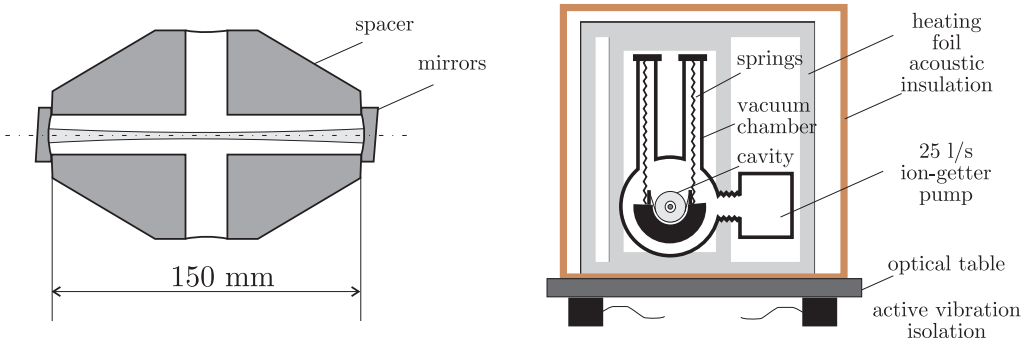

FIG. 1: *(left) — Reference cavity for stabilization of the dye laser at 486 nm. The cavity spacer is oriented horizontally and is supported from the bottom. (right) — The cavity assembly (not to scale) is placed in the vacuum chamber with two stages of temperature stabilization. The total volume of the device is about 3 m^3.*

width of the dye laser has been measured to be 60 Hz for averaging times of 0.2 s [27]. The long-term drift of the cavity, measured over 5 years relative to the $1S-2S$ transition frequency in atomic hydrogen, is about +0.05 Hz/s which most likely derives from aging of the ULE spacer. The stabilized dye laser at 486 nm turned out to be a powerful and reliable light source. Its radiation is frequency doubled in a barium β-borate crystal (BBO). All experiments on hydrogen which will be presented in this chapter have been made using this dye laser.

The diode laser source is a frequency-quadrupled master-oscillator power-amplifier system [24]. A laser diode operating at 972 nm is placed in an external Littrow cavity. The output is amplified using a tapered amplifier (TA), producing 650 mW at 972 nm. A small fraction of this light is used for stabilization to an external reference cavity. In this case we used an elaborated concept of a vertical mid-plane reference cavity [28] which provides over 40 dB less sensitivity to vertical vibrations [29]. Its 7.5 cm spacer is made from selected ULE material and is commercially available [30]. The principle of vibration suppression is illustrated in Fig. 2, where the calculated deformation of such a cavity under acceleration of 1 g is presented. By design the top and bottom parts of the cavity, where the cavity mirrors are located, deform in a synchronized way such that the distance between the mirrors, which defines the optical resonance, is maintained under vertical acceleration induced by seismic or acoustic vibrations.

We have measured a finesse $\mathcal{F} = 420\,000$ at 972 nm of the two vertical cavities which are at our disposal using the standard ringdown method. The first cavity is placed in an aluminum vacuum chamber which is pumped by a small 2 l/s ion-getter pump to 10^{-7} mbar. The chamber and the pump are temperature stabilized by a conventional integrating servo circuit. Another stage of temperature and acoustic isolation consists of a hermetically sealed aluminum

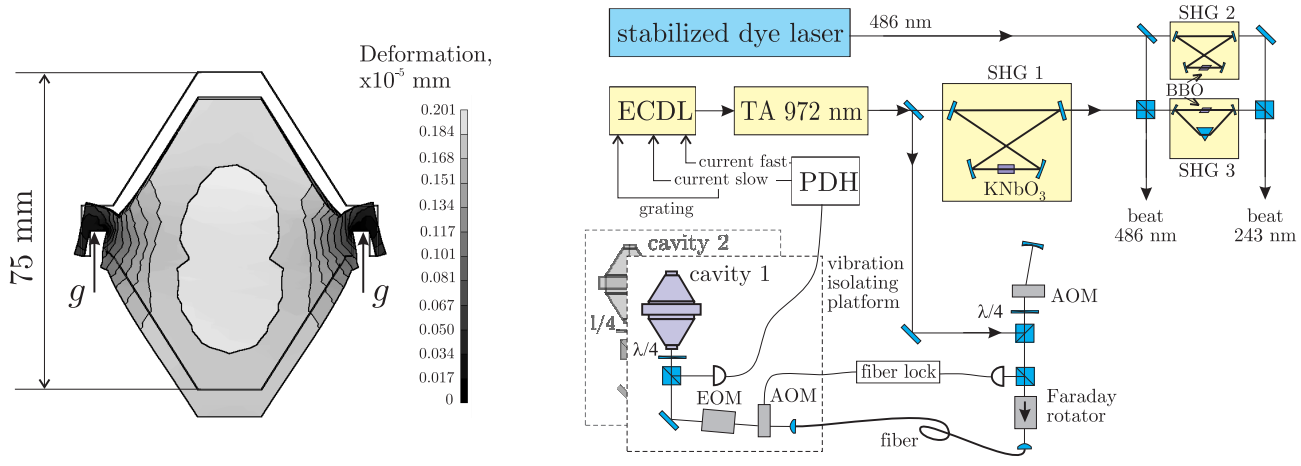

FIG. 2: *(left) — Calculated deformation of a mid-plane supported 2-D glass block with a cross section of our vertical cavity under acceleration of 1 g. (right) — Stabilization of the external cavity diode laser (ECDL) at 972 nm to the vertical reference cavity. To characterize the spectral properties of the laser system we either use the Pound-Drever-Hall error signal from the second reference cavity or the radiation from the stabilized dye laser at 486 nm.*

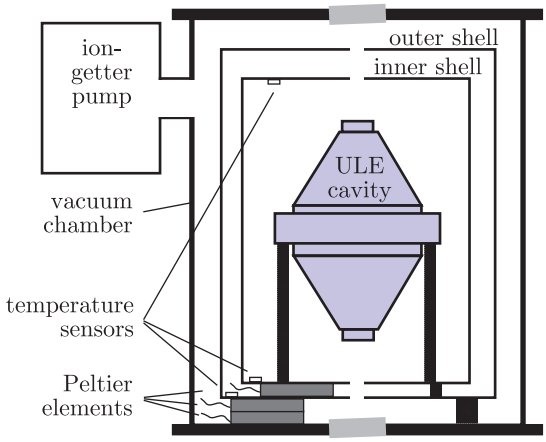

FIG. 3: *Reference cavity "matryoshka-design". The cavity temperature can be stabilized from 7° C to 20° C by Peltier elements. The shells are made from aluminum. A free running sensor (at the top) detects temperature fluctuations in the range of 2 mK correlated with fluctuations of the laboratory air conditioning system.*

box, each side of which is controlled by a two-point relay temperature stabilization system providing uniform radiation temperature from all sides to the vacuum chamber. The optical ports are equipped with narrow-band interference filters. Temperature fluctuations on the walls of the vacuum chamber do not deviate by more than 1 mK from the set temperature of 31 °C on a time sale of a few hours. In comparison to the 486 nm cavity setup, the volume is significantly reduced to less then 0.04 m^3.

Relative length changes of ULE show a temperature dependence of $\delta\ell/\ell \sim 10^{-9}(T - T_c)^2\,\mathrm{K}^{-2}$ [29], where T_c is the zero-expansion temperature at which the spacer reaches its minimum length. So far T_c could not be specified reliably by the manufacturer and turns out slightly below room temperature. To measure T_c and to characterize the spectral properties, a second cavity with a vertical oriented axis has been constructed. To be able to reach the zero expansion temperature this cavity must be cooled below room temperature. This is achieved by placing it inside two nested cylindrical aluminum shells ("matryoshka-design"), both of which housed in a vacuum vessel. The inner shell is thermally coupled to the outer one by a Peltier element, while the latter is coupled to the internal surface of the stainless steel vacuum chamber by another double-stage Peltier element. Each of the shells has its individual temperature control unit. The vacuum system is pumped out by a 25 l/s ion-getter pump to 10^{-7} mbar. This configuration allowed us to cool the second cavity to 7 °C with temperature fluctuations of the inner shell of about 2 mK. Due to the reduced thermal insulation, temperature coupling to the environment and the corresponding time constant are worse for this system in comparison with the room temperature cavity. Results of T_c measurement are presented below.

Both 972 nm cavities are placed on separate active vibration-isolating platforms and equipped with Pound-Drever-Hall feedback systems each of which consisting of a temperature-stabilized electro-optical modulator (EOM), a fast photo-diode and necessary optics (see Fig. 2 (right)). The light from the laser is coupled to each cavity by a single-mode optical fiber (cleaved at 8 ° at the exit side), with the standard fiber-noise cancellation method applied [31]. The diode laser is locked to one of the vertical cavities, while the error signal from the second cavity is used to investigate the spectral properties of the stabilized diode laser. We also measured a beat note between the stabilized dye laser at 486 nm and the frequency-doubled light from the diode laser system which allowed us to separately investigate fast phase noise fluctuations of the diode laser.

As shown on the right hand side of Fig. 2, the dye laser as well as the radiation of the doubled diode laser are frequency doubled once again in separate second harmonics generation stages (SHGs 2 and 3). After astigmatism compensation both systems yield about 20 mW narrow-band radiation at 243 nm in near-Gaussian beams. In addition to the beat note at 486 nm we also generate a beat signal at 243 nm for closer investigation of the spectral characteristics.

The beat note power spectrum between the dye laser and the second harmonic of the diode laser is presented in Fig. 4 (left) for large frequency detunings. One observes a narrow central peak on a broad pedestal of a few MHz spectral width. We ascribe the origin of this pedestal to uncompensated high-frequency phase noise of the diode laser and to phase noise of its electronic feedback loop [32]. Indeed, the main contribution of the phase noise of the free-running dye laser is due to low-frequency acoustic vibrations and can be suppressed very efficiently. The assumption, that the main contribution to the pedestal is due to the diode laser radiation can be readily tested by

changing the parameters of the corresponding feedback loops: It turns out that the pedestal shape is very sensitive to the adjustment of the diode laser feedback. Obviously for such a line shape (narrow peak sitting on a broad pedestal) the line width is not a very useful concept. To characterize the spectrum we rather measure the relative power contained in the narrow central peak.

This fractional power reaches $S_{486} = 0.95$ for proper adjustment of the diode laser electronic feedback. Following Ref. [25], the power fraction in the central peak can be written as:

$$S = e^{-\langle\phi^2\rangle}\,, \tag{1}$$

which is valid not only for the case of small modulation depth, but also for deep modulation $\langle\phi^2\rangle \sim 1$. Here ϕ is the rms phase noise of the laser radiation which is assumed to correspond to a Gaussian distributed ergodic noise process. From the last equation one finds, that doubling the rms phase noise that takes place when doubling the laser frequency, reduces the fractional power of the central peak to:

$$S' = S^4\,. \tag{2}$$

This reduction not only applies to the second harmonic generation steps but effectively also for driving a two-photon transition. The carrier reduction process is illustrated in Fig. 4 (right), where the power spectrum of the beat signal at 243 nm between the second harmonic of the dye laser and the fourth harmonic of the diode laser is presented. The power fraction of the carrier is reduced in agreement with (2) to $0.95^4 = 0.81$. From this we conclude that the rms phase noise of the diode laser at 972 nm to be $\phi = 6.5\,^\circ$ and that we can expect a carrier strength of the $1S-2S$ transition to be 44%. This underlines the importance of putting as much power as possible into the carrier of the diode laser with a proper cavity locking system.

More information from the beat note spectra can be obtained by analyzing the line shape of the carrier in addition to its fractional power. It can be shown, that the spectral line width of an oscillator is doubled or quadrupled in a frequency doubling process (SHG or two-photon transition) depending on the noise properties of the oscillator [34, 35]. The two cases are fast short-correlated phase variation with small amplitude and long-correlated phase variation with large amplitude. Let us consider an oscillator output $A_0\cos(\omega_0 t + \varphi(t))$, where ω_0 is the carrier frequency and $\varphi(t)$ is the fluctuating phase. Frequency fluctuations $\Omega(t) = \dot{\varphi}(t)$ are assumed to correspond to a stationary stochastic process having an rms amplitude of $\Omega_{\rm rms}$ and correlation time of τ_Ω. The two types of modulations can be distinguished from their line shape and frequency doubling properties. Short-correlated phase noise ($\Omega_{\rm rms}\tau_\Omega \ll 1$) produces a Lorentzian shape whose width is quadrupled when doubling the carrier frequency. On the other hand deep slow phase variations ($\Omega_{\rm rms}\tau_\Omega \gg 1$) produce Gaussian line shapes, that only double in width after frequency doubling.

By zooming into the central part of the beat note spectrum we compared the spectral line widths at 486 nm and 243 nm (Fig. 4) and observed, that the spectral width doubles after the second SHG stage. This indicates that the residual line width of the stabilized dye laser results from slow but large phase excursions. A good fraction of that noise origins from the horizontal cavity suspension to which the dye laser is locked (Fig. 1) which has an eigenfrequency of about 1 Hz. We measured the spectral width of the central peak to be 60 Hz for averaging times of 0.4 s. Frequency fluctuations of the stabilized diode laser are negligible on this time scale because its vertical reference cavity does not sway. This evaluation of the spectral line width of the dye laser is independently confirmed by measurements of the spectral width of the $1S-2S$ transition [33].

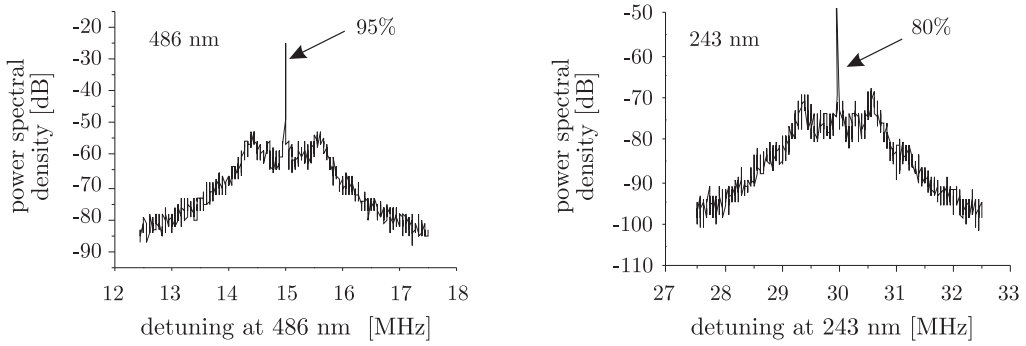

FIG. 4: *(left) — Power spectral density of the beat signal at 486 nm between the second harmonic of the stabilized diode laser and stabilized dye laser. (right) — Simultaneously recorded spectrum of the beat signal at 243 nm. The fraction of power of the central peak relative to the total power is given as a percentage in the plots.*

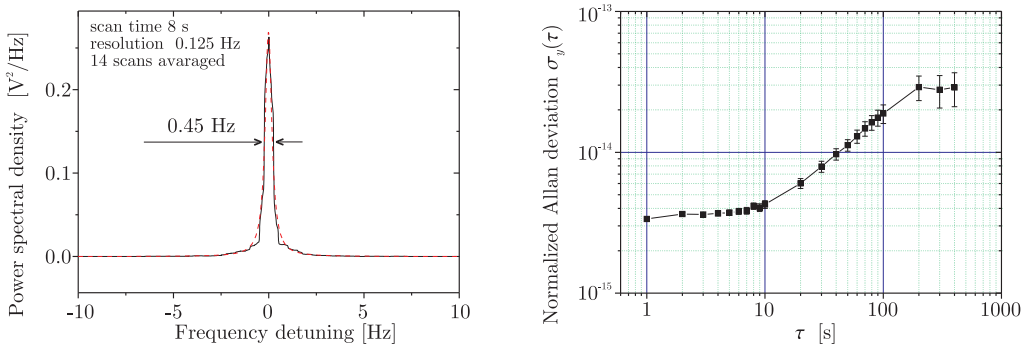

FIG. 5: *(left) — Power spectrum of the beat signal between two independent 972 nm vertical cavities supported at mid plane. The data is obtained from drift corrected average of 14 consecutive spectra recorded with a the scan time of 8 s and a resolution of the FFT spectrum analyzer of 0.125 Hz. The dashed line is a Lorentzian fit to the data. (right) — Normalized Allan deviation for these cavities. Linear drift has been subtracted.*

To investigate the stability of our vertical 972 nm cavities we used one of the cavities as frequency discriminator while locking the diode laser system to the other cavity. Due to small drift rate of the cavities one can either directly analyze the error signal generated by the discriminator cavity or by using this signal to lock an AOM shifted copy of the diode laser output [36]. In the latter case the spectrum of the beat note between the two decoupled light fields is analyzed. Only noise components inside the AOM locking servo bandwidth (a few tens of kilohertz) are properly reproduced in this way. A typical power spectrum of such a beat note is presented in Fig. 5 (left). It has been recorded by an FFT spectrum analyzer with a resolution of 0.125 Hz and a scan time of 8 s. The plot is an average of 14 sequential scans where the drift induced shift of the beat note is corrected for. The spectral line shows a Lorentzian shape with a 0.45 Hz full width at a half maximum.

The typical relative drift of two vertical 972 nm cavities corresponds to about 1 Hz/s and results mostly from temperature fluctuations of the cavities and the EOM crystals which causes the lock point of the Pound-Drever-Hall stabilization to drift. A plot of the Allan deviation of the frequency difference of the two vertical cavities is presented in Fig. 5 (right).

To determine the ULE zero expansion point T_c we have measured the frequency of the beat note between the two vertical cavities while varying the temperature of the Peltier-controlled matryoshka-design. The second vertical cavity served as a frequency reference with a negligible long-term drift. After changing the set temperature we waited for about one day to reach the new equilibrium before the beat note frequency was measured. The result is shown in Fig. 6 (left).

One observes a parabolic dependence which corresponds to the expected ULE thermal expansion. At $T_c \approx 12.5\,^{\circ}\mathrm{C}$

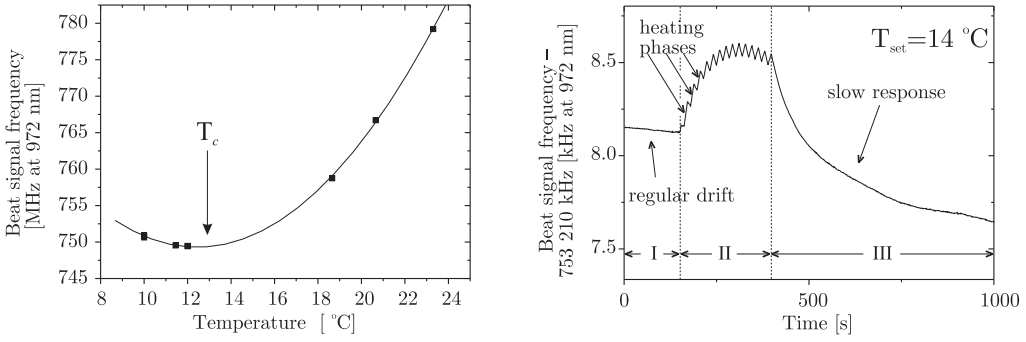

FIG. 6: *(left) — Measurement of the cavity zero expansion temperature T_c. Note, that linear thermal expansion of the multilayer coating significantly contributes to the cavity length changes which results in a shift of measured value for T_c with respect to the zero expansion point of pure ULE glass material. (right) — Cavity response to modulated heating. During the period I the background drift rate is observed. For period II a modulated heating laser is periodically switched on which homogenously illuminated the cavity through the viewport of the vacuum chamber. In period III the heating is turned off and the cavity returns to the slow thermal response of the mirror substrates and the spacer, both made from ULE.*

the distance between mirrors reaches its minimum and so does the beat note frequency. By choosing the working point at T_c, one could expect a minimal sensitivity to temperature fluctuations. Exactly at T_c the spacer length fluctuations become negligible in comparison with thermal response of the multilayers coating which in our case has a thickness of 5 μm on each mirror. The result of the coating thermal expansion is observed in Fig. 6 (right). In this simple experiment we heat the cavity through the vacuum viewport using the radiation of a 830 nm fiber-coupled laser diode emitting about 30 mW in a wide solid angle. The light of the diode has been periodically switched on and off for 10 s intervals.

We ascribe a fast response of the cavity resonance frequency to laser heating to thermal expansion of the multilayer mirror coatings [37]. After switching off the light one can observe the coating and the substrate thermalizing with the spacer in few hundred seconds, and the spacer starts slowly to react by changing its length (the experiment has been performed at $T > T_c$). By quickly changing the temperature of the aluminum shell surrounding the cavity, through one of the Peltier elements, we have estimated the sensitivity of its resonance frequency to blackbody radiation to about 3 Hz/mK. Thus, even if working at T_c one has to suppress fast temperature fluctuations and carefully shield the cavity from external radiation sources which can cause short-term cavity length fluctuations and loss of stability. On the other hand, working near T_c allows to suppress long-term cavity drift.

For routine measurements of the $1S-2S$ transition in atomic hydrogen we still use the dye laser system. Though it possesses significantly broader spectral carrier line width (60 Hz at 486 nm in comparison with sub-hertz line width of the diode laser system), the fraction S of the power falling in the narrow carrier approaches 1 which allows for more efficient excitation of atomic hydrogen. It should be noted that the observed $1S-2S$ transition line width is still significantly larger than 60 Hz (measured at 486 nm). Therefore the dye laser allows to model the hydrogen line shape based on fundamental physics rather than modelling the line shape of the exciting laser. This is important for the ability to split the observed line width in order to derive a precise value for the unperturbed transition frequency. However, the laser diode system may become useful for the $1S-2S$ transition after increasing the finesse of the enhancement cavity at 243 nm (see below) and/or further improving the diode laser locking scheme.

B. Hydrogen spectrometer

To efficiently excite the $1S-2S$ two-photon transition in atomic hydrogen it is necessary to illuminate the atoms by intense laser radiation at 243 nm. A resonance line independent of the Doppler shift to first order is obtained by using two counter propagating laser beams for that purpose. The conditions for this excitation scheme are fulfilled by employing an enhancement cavity as shown in Fig. 7. The cavity consists of a flat input coupling mirror and a concave output coupling mirror (radius $R = -4$ m) separated by a distance of about 30 cm.

Atomic hydrogen is produced in a microwave gas discharge and emerges from a copper nozzle cooled by a flow-through helium cryostat to $T \simeq 5$ K. Thermalized atoms escape the nozzle of 1 – 2 mm in diameter and enter the interaction zone co-linear with the laser beam. The atomic beam is restricted by two diaphragms (not shown in Fig. 7). We operate at a typical gas flow of 4×10^{17} particles per second with an estimated 10% dissociated atomic fraction. During the flight through the Gaussian profile of the cavity TEM_{00} mode, some of the atoms are promoted to the metastable $2S$ state. When entering the Lyman-α detector these atoms are quenched in a weak dc electric field. This field mixes the $2S$ state with the short-lived $2P$ state causing the prompt emission of a Lyman-α photon which is detected by a photomultiplier tube. After the 1999 measurement, which had been performed at a background gas pressure of around 10^{-6} mbar, we have upgraded the vacuum system by supplying it with a differential pumping configuration that separates a high vacuum (HV) from an ultra high vacuum section (UHV). This allowed us to vary the background gas pressure between 10^{-8} and 10^{-7} mbar in the 2003 measurement to deduce the background gas pressure shift and to reduce the corresponding uncertainty down to 2 Hz.

To limit the velocity of atoms contributing to the signal in order to reduce velocity-dependent systematic effects, a time-of-flight detection scheme is used. For this purpose the excitation laser is chopped by a wheel chopper operating at 160 Hz with a 50% duty cycle. A sharp trigger signal is generated each time when the 3 ms dark phase starts. Then, a precisely defined time delay $\Delta\tau$ is introduced between the trigger and the start of the detection of the Lyman-α signal. After that, the photon accumulation continues until the end of the dark chopper phase. By using this technique, all atoms with velocities larger than $v_{\max}(\Delta\tau) = \ell_{\rm int}/\Delta\tau$ escape the detection zone of length $\ell_{\rm int} \approx 14$ cm (the distance separating the nozzle and the photomultiplier) before the start of the detection cycle and do not contribute. Another advantage of this technique is a significant suppression of the background count rate originating from scattered 243 nm light that would otherwise be registered by the photomultiplier.

To record a hydrogen resonance line the laser frequency is scanned stepwise across the resonance while a multichannel scaler records the number of detected Lyman-α photons for 12 different delays $\Delta\tau_i = 10,\ 210,\ 410,\ \ldots,\ 2210\ \mu s$ in the corresponding time windows $\{\Delta\tau,\ 3\ \text{ms}\}$. The accumulation time for each laser frequency setting is one second and typically about 50 different detunings are collected to record a hydrogen time-resolved spectrum.

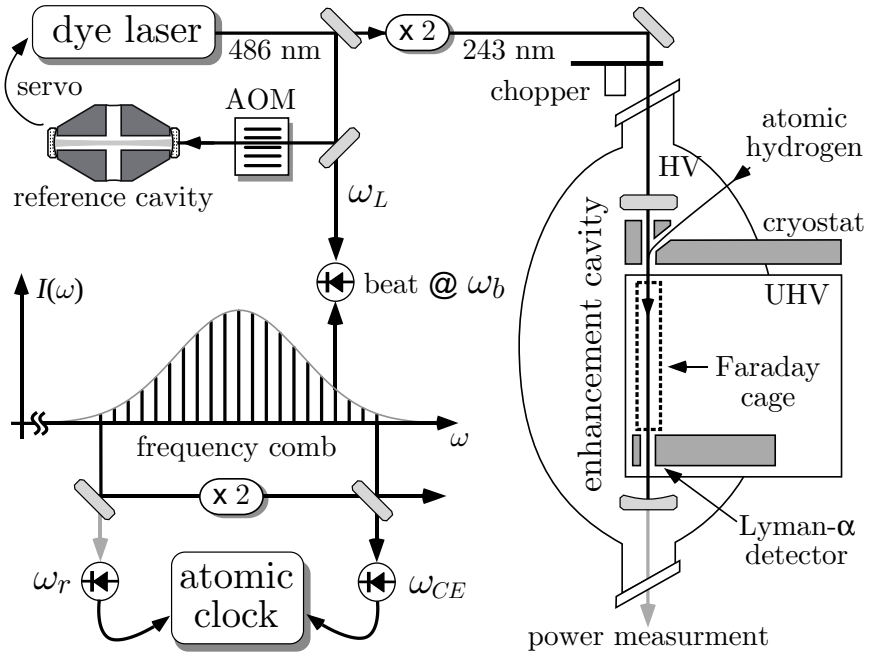

FIG. 7: *The hydrogen spectrometer. The frequency ω_L of the light from the dye laser is measured with a frequency comb locked to a primary frequency standard while the same light is used to excite the $1S-2S$ transition in a beam of atomic hydrogen. See text for further details. Details on the frequency comb are given in Section III.*

The radiation transmitted trough the enhancement cavity is monitored by a calibrated silicon photodiode. The photodiode readout is averaged over the laser frequency dwelling time to normalize the spectrum and determine the ac Stark shift. Dividing the photodiode readout by the transmission of the output coupling mirror we get the total power circulating in the enhancement cavity per direction.

Using this detection technique we simultaneously record 12 lines, each containing the contributions of atoms in the respective velocity range $0 < v < v_{\max}(\Delta\tau_i)$ $(i = 1, \ldots, 12)$, selected from the same initial velocity distribution $f(v)$. Following Ref. [38] the velocity distribution of a one-dimensional thermal atomic beam effusing from thermalized gas volume through a hole in a thin wall is given by:

$$f(v) \propto (v/v_0)^3 \exp[-(v/v_0)^2]\,, \tag{3}$$

where $v_0 = \sqrt{2k_BT/m_{\rm H}}$ is the most probable thermal velocity for a given temperature T and $m_{\rm H}$ is the mass of the hydrogen atom. As discussed in [38] and references therein, expression (3) is valid for perfectly collimated beams and should be further modified in other cases. The collimation angle of the atomic beam in our experiment is about 0.01 which justifies the use of $f(v)$ for modelling.

A large delay $\Delta\tau$ reduces the maximum velocity $v_{\max}(\Delta\tau)$ of atoms contributing to the signal, which is desired, but also decreases the Lyman-α count rate. The slow atoms contribution show a small time-of-flight broadening and a small second-order Doppler effect so that a narrow and symmetric transition line shape is obtained. Hence, the fast atoms provide good statistics whereas the slow atoms show superior systematics. For a highly accurate measurement we need to combine good statics with low systematics. For this reason we have developed a detailed line-shape model [19] that can use all delays by taking into account all dynamic effects associated with the movement of the hydrogen atoms through the laser beam.

A typical time-resolved spectrum of the $1S-2S$ transition is shown in Fig. 8. The most important systematic effects that shift the transition frequency are the 2nd order Doppler effect and the ac Stark shift. The latter reads $\Delta\nu_{\rm AC} = 2\beta_{\rm AC} I(\vec{r})$, where $I(\vec{r})$ is the intensity of the laser beam at position $\vec{r}$ per direction with $\beta_{\rm AC} = 1.67\,{\rm Hz}\,({\rm W/cm^2})^{-1}$ [21]. The value for ac Stark shift averaged over the atomic trajectories is in the range of $0.1-1\,$kHz for our experimental excitation intensities. To determine the unperturbed transition frequency we measure at different intensities and extrapolate to zero intensity. There are other small systematic effects like the dc Stark shift, the pressure shift, the blackbody shift to name a few, that contribute on the level of a few hertz.

Three different effects are the main contribution to the observed $1S-2S$ line width (see Fig. 8 (right)): Time of flight broadening, power broadening and ionization broadening that add in highly non-trivial way [33]. For lower

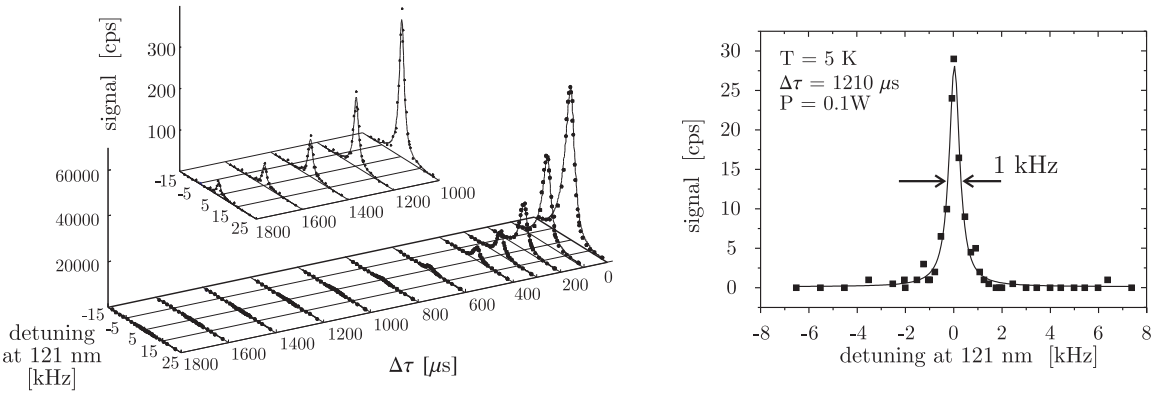

FIG. 8: *(left) — Experimental time-resolved spectrum of the* $1S-2S$ *transition together with a fit obtained from a line shape model (solid lines) [19]. (right) — Typical transition line detected at low excitation power circulating in the enhancement cavity (the on-axis intensity* $I(0)$ *per direction of 200* W/cm^2*) and a time delay* $\tau = 1210\,\mu s$*.*

excitation powers and delay times of about 1 ms the resolution of the hydrogen spectrometer reaches 2×10^{13}. To measure the frequency of the $1S-2S$ transition a small part of 486 nm light is sent to an octave-spanning frequency comb referenced to a primary frequency standard (see Fig. 7). The principles of operation of the frequency comb along with results of the $1S-2S$ transition frequency measurements will be given in the following Section.

III. OPTICAL FREQUENCY MEASUREMENTS

Frequency can be measured with by far the highest precision of all physical quantities. In the radio frequency (rf) domain (say up to 100 GHz), frequency counters have existed for a long time. Almost any of the most precise measurements in physics have been performed with such a counter that uses an atomic clock as a time base. To extend this accurate technique to higher frequencies, so called harmonic frequency chains have been constructed since the late 1960ies [39, 40]. In such a chain nonlinear elements produce frequency multiples (harmonics) of a given oscillator to which a subsequent oscillator is phase locked to. The latter is necessary because nonlinear devices usually produce only weak signals, at least when they are driven with a continuous wave. Electronic phase locked loops can be used to stabilize any kind of oscillator, even lasers, provided their intrinsic stability is sufficient so that there is no need for very rapid frequency corrections. Repeating the multiply and phase lock procedure many times makes it possible to convert a reference radio frequency, say from an atomic clock, to much higher frequencies. Because of the large number of steps necessary to build a long harmonic frequency chain, it was not before 1995 when visible laser light was first referenced phase coherently to a cesium atomic clock using this method [41].

The disadvantage of these harmonic frequency chains was not only that they could easily fill several large laser laboratories at once, but that they could be used to measure a single optical frequency only. Even though mode locked lasers for optical frequency measurements have been used in rudimentary form in the late 1970ies [42], this method became only practical with the advent of femtosecond (fs) mode locked lasers. Such a laser necessarily emits a very broad spectrum, comparable in width to the optical carrier frequency. Currently the working horse in that field is the titanium-sapphire Kerr-lens mode locked laser, but fiber based lasers are expected to take over for frequency metrology applications. Omitting exciting, but involved history of the development of octave-spanning frequency combs, we will restrict ourselves to the description of its principles of operation using as an example the most recent absolute frequency measurements of the $1S-2S$ transition in atomic hydrogen.

A. Ultra-short pulse lasers and frequency combs

In the frequency domain a train of short pulses from a femtosecond mode locked laser is the result of a phase coherent superposition of many continuous wave (cw) longitudinal cavity modes. These modes at ω_n form a series of frequency spikes that is called a frequency comb. The individual modes can be selected by phase locking other cw lasers to them. As has been shown, the modes are remarkably uniform, i.e. the separation between adjacent modes is constant across the frequency comb [10, 12, 43, 44]. This strictly regular arrangement is the most important feature

used for optical frequency measurement and may be expressed as:

$$\omega_n = n\omega_r + \omega_{CE}\,. \tag{4}$$

Here the mode number n of some 10^5 may be enumerated such that the frequency offset ω_{CE} lies in between 0 and $\omega_r = 2\pi/T$. The mode spacing is thereby identified with pulse repetition rate, i.e. the inverse pulse repetition time T. With the help of that equation two radio frequencies ω_r and ω_{CE} are linked to the optical frequencies ω_n of the laser. For this reason mode locked lasers are capable to replace the harmonic frequency chains of the past.

To derive the frequency comb properties [45] as detailed by (4), it is useful to consider the electric field $E(t)$ of the emitted pulse train. We assume that the electric field $E(t)$, measured for example at the lasers output coupling mirror, can be written as the product of a periodic envelope function $A(t)$ and a carrier wave $C(t)$:

$$E(t) = A(t)C(t) + c.c.\,. \tag{5}$$

The envelope function defines the pulse repetition time $T = 2\pi/\omega_r$ by demanding $A(t) = A(t-T)$. The only thing about dispersion that should be added for this description, is that there might be a difference between the group velocity and the phase velocity inside the laser cavity. This will shift the carrier with respect to the envelope by a certain amount after each round trip. The electric field is therefore in general not periodic with T. To obtain the spectrum of $E(t)$ the Fourier integral has to be calculated:

$$\tilde{E}(\omega) = \int_{-\infty}^{+\infty} E(t)e^{i\omega t}dt\,. \tag{6}$$

Separate Fourier transforms of $A(t)$ and $C(t)$ are given by:

$$\tilde{A}(\omega) = \sum_{n=-\infty}^{+\infty} \delta\left(\omega - n\omega_r\right)\tilde{A}_n \qquad \text{and} \qquad \tilde{C}(\omega) = \int_{-\infty}^{+\infty} C(t)e^{i\omega t}dt\,. \tag{7}$$

A periodic frequency chirp imposed on the pulses is accounted for by allowing a complex envelope function $A(t)$. Thus the "carrier" $C(t)$ is defined to be whatever part of the electric field that is non-periodic with T. The convolution theorem allows us to calculate the Fourier transform of $E(t)$ from $\tilde{A}(\omega)$ and $\tilde{C}(\omega)$:

$$\tilde{E}(\omega) = \frac{1}{2\pi}\int_{-\infty}^{+\infty} \tilde{A}(\omega')\tilde{C}(\omega-\omega')d\omega' + c.c. = \frac{1}{2\pi}\sum_{n=-\infty}^{+\infty} \tilde{A}_n\tilde{C}\left(\omega - n\omega_r\right) + c.c.\,. \tag{8}$$

The sum represents a periodic spectrum in frequency space. If the spectral width of the carrier wave $\Delta\omega_c$ is much smaller than the mode separation ω_r, it represents a regularly spaced comb of laser modes just like (4), with identical spectral line shapes, namely the line shape of $\tilde{C}(\omega)$ (see Fig. 9). If $\tilde{C}(\omega)$ is centered at say ω_c, than the comb is shifted from containing only exact harmonics of ω_r by ω_c. The center frequencies of the mode members are calculated from the mode number n [11, 42, 45]:

$$\omega_n = n\omega_r + \omega_c\,. \tag{9}$$

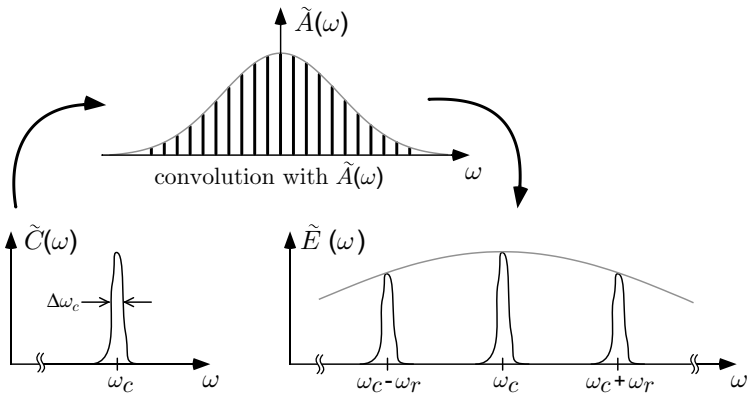

FIG. 9: The spectral shape of the carrier function (left), assumed to be narrower than the pulse repetition frequency ($\Delta\omega_c \ll \omega_r$), and the resulting spectrum according to (8) after modulation by the envelope function (right).

The measurement of the frequency offset ω_c as described below (see also [10, 11, 43, 45, 47]) usually yields a value modulo ω_r, so that renumbering the modes will restrict the offset frequency to smaller values than the repetition frequency and (4) and (9) are identical.

If the carrier wave is monochromatic $C(t) = e^{-i\omega_c t - i\varphi}$, its spectrum will be δ-shaped and centered at the carrier frequency ω_c. The individual modes are also δ-functions $\tilde{C}(\omega) = \delta(\omega - \omega_c)e^{-i\varphi}$. The frequency offset (9) is identified with the carrier frequency. According to (5) each round trip will shift the carrier wave with respect to the envelope by $\Delta\varphi = \arg(C(t-T)) - \arg(C(t)) = \omega_c T$ so that the frequency offset may also be identified by $\omega_{CE} = \Delta\varphi/T$ [11, 42, 45]. In a typical laser cavity this pulse-to-pulse carrier-envelope phase shift is much larger than 2π, but measurements usually yield a value modulo 2π. The restriction $0 \leq \Delta\varphi \leq 2\pi$ is synonymous with the restriction $0 \leq \omega_{CE} \leq \omega_r$ introduced above. Fig. 10 sketches this situation in the time domain for a chirp free pulse train.

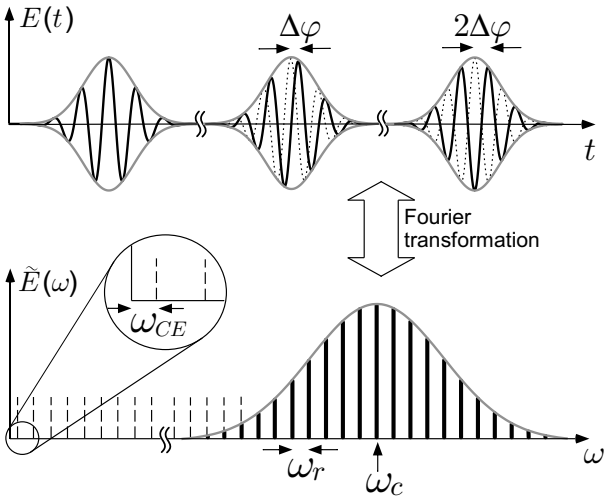

FIG. 10: *Consecutive un-chirped pulses ($A(t)$ is real) with carrier frequency ω_c and the corresponding spectrum (not to scale). Because the carrier propagates with a different velocity within the laser cavity than the envelope (with phase- and group velocity respectively), the electric field does not repeat itself after one round trip. A pulse-to-pulse phase shift $\Delta\varphi$ results in an offset frequency of $\omega_{CE} = \Delta\varphi/T$. The mode spacing is given by the repetition rate ω_r. The width of the spectral envelope is given by the inverse pulse duration up to a factor order unity that depends on the pulse shape.*

In a real laser the carrier wave will not be a clean sine wave as in this example. The mere periodicity of the field, allowing a pulse to pulse carrier envelope phase shift, already guarantees the comb like spectrum. Very few effects can disturb that property. In particular, for an operational frequency comb, both ω_r and ω_{CE} will be servo controlled so that slow drifts are compensated. The property that the comb method really relies on, is the mode spacing being constant across the spectrum. Even a small deviation from this condition will have very quick and devastating effects on the pulse envelope. However, the phase of individual modes can fluctuate about an average value required for staying in lock with the rest of the comb.

B. Extending the frequency comb

The spectral width of a pulse train emitted by a fs laser can be significantly broadened in a single mode fiber [46] by self phase modulation. Assuming a single mode carrier wave, a pulse that has propagated the length L acquires a self induced phase shift of

$$\Phi_{NL}(t) = -n_2 I(t)\omega_c L/c\,, \tag{10}$$

where the pulse intensity is given by $I(t) = \frac{1}{2}c\varepsilon_0|A(t)|^2$. For fused silica the non-linear Kerr coefficient n_2 is comparatively small but almost instantaneous even on the time scale of fs pulses. This means that different parts of the pulse travel at different speed. The result is a frequency chirp across the pulse without affecting the its duration. The pulse is no longer at the Fourier limit so that the spectrum is much broader than the inverse pulse duration where the extra frequencies are determined by time derivative of the self induced phase shift $\dot{\Phi}_{NL}(t)$. Therefore pure self-phase modulation would modify the envelope function in (5) according to

$$A(t) \longrightarrow A(t)e^{i\Phi_{NL}(t)}. \tag{11}$$

Because $\Phi_{NL}(t)$ has the same periodicity as $A(t)$ the comb structure of the spectrum is maintained and the derivations (8) remain valid because periodicity of $A(t)$ was the only assumption made. An optical fiber is most appropriate for this process because it can maintain the necessary small focus area over a virtually unlimited length. In practice, however, other pulse reshaping mechanism, both linear and non-linear, are present so that the above explanation is too simple.

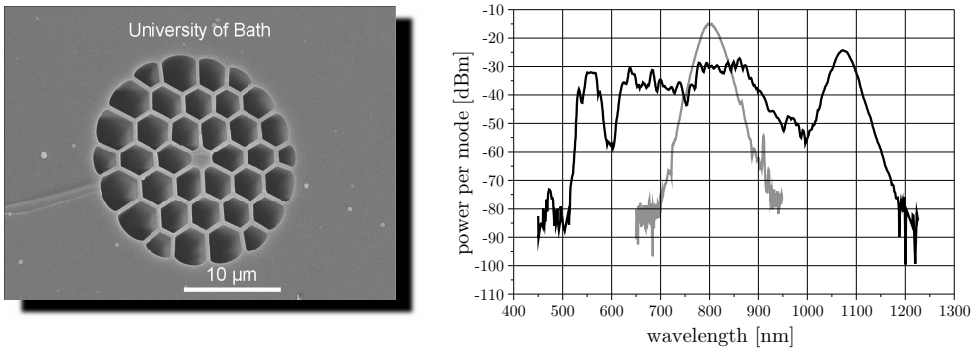

FIG. 11: *(left) — SEM image of a the core of a microstructure fiber made at the University of Bath, UK [48]. The light is guided in the central part but the evanescent part of the wave penetrates into the air holes that run parallel to the fiber core and lower the effective refractive index without any doping. The guiding mechanism is the same as in a conventional single mode fiber. (right) — Power per mode on a logarithmic scale (0 dBm = 1mW). The lighter 30 nm (14 THz at −3 dB) wide spectrum displays the laser intensity and the darker octave spanning spectrum (532 nm through 1064 nm) is observed after the microstructure fiber that was 30 cm long. The laser was operated at $\omega_r = 2\pi \times 750$ MHz (modes not resolved) with 25 fs pulse duration. An average power of 180 mW was coupled through the microstructure fiber [52].*

Higher order dispersion is usually limiting the effectiveness of self phase modulation as it increases the pulse duration and therefore lowers the peak intensity after a propagation length of a few mm or cm for fs pulses. On can get a better picture if pulse broadening due to group velocity dispersion $k''(\omega_c)$ is included. To measure the relative importance of the two processes, the dispersion length L_D (the length that broadens the pulse by a factor $\sqrt{2}$) and the non-linear length L_{NL} (the length that corresponds to the peak phase shift $\Phi_{NL}(t=0)=1$) are used [46]:

$$L_D = \frac{4\ln(2)\tau_0^2}{|k''(\omega_c)|}\,, \qquad L_{NL} = \frac{cA_f}{n_2\omega_c P_0}\,, \tag{12}$$

where τ_0, A_f and $P_0 = \frac{1}{2}A_f c\varepsilon_0|A(t=0)|^2$ are the initial pulse duration, the effective fiber core area and the pulse peak power respectively. In the dispersion dominant regime $L_D \ll L_{NL}$ the pulses will disperse before any significant nonlinear interaction can take place. On the other hand, for $L_D > L_{NL}$ spectral broadening could be thought as effectively taking place for a length L_D even though the details are more involved. The total non-linear phase shift can therefore be approximated by the number of non-linear lengths within one dispersion length. As this phase shift occurs roughly within one pulse duration τ_0, the spectral broadening is estimated to be $\Delta\omega_{NL} = (L_{NL}/L_D)\tau_0^{-1}$. As an example consider a silica single mode fiber (Newport F-SF) with $A_f = 26\ \mu\text{m}^2$, $k''(\omega_c) = 281$ fs/cm^2 and $n_2 = 3.2\times10^{-16}$ cm^2/W that is seeded with $\tau_0 = 73$ fs Gaussian pulses (FWHM intensity) at 905 nm with 225 mW average power and a repetition rate of 76 MHz [45, 51]. In this case the dispersion length becomes 6.1 cm and the non-linear length 35 mm. The expected spectral broadening of $(L_{NL}/L_D)\tau_0^{-1} = 2\pi \times 44$ THz is indeed very close to the observed value [45].

It turns out that within this model the spectral broadening is independent of the pulse duration τ_0 because $P_0 \propto \tau_0$. Therefore using shorter pulses may not be effective for extending the spectral bandwidth beyond an optical octave as required for simple self-referencing (see the next Section). However, very efficient spectral broadening can be obtained in microstructure fiber[120] that can be manufactured with $k''(\omega_c) \approx 0$ around a design wavelength [48–50]. In this case the pulses are broadened by other processes (linear and non-linear) than group velocity dispersion as they propagate along the fiber. Eventually this will also terminate self phase modulation and the dispersive length has to be replaced appropriately in the above analysis. At this point a whole set of effects enter such as Raman and Brillouin scattering, optical wave breaking and modulation instability [46]. Some of these processes even spoil the usefulness of the broadened frequency combs as they amplify noise.

A microstructure fiber uses an array of submicron-sized air holes that surround the fiber core and run the length of a silica fiber to obtain a desired effective dispersion. This can be used to maintain the high peak power over

an extended propagation length and to significantly increase the spectral broadening. With these fibers it became possible to broaden low peak power, high repetition rate lasers to beyond one optical octave as Fig. 11 shows.

Even though microstructure fibers have been very useful to spectrally broaden frequency comb, coupling to its tiny core can cause problems due to mechanical instabilities and temperature drifts even with low level and stable mounts. Another problem with spectral broadening by self phase modulation that it typically results in an excess noise level of the beat notes well above the shot noise limit [57, 58]. Meanwhile lasers that reach an octave spanning spectrum without using any external self-phase modulation can solve this problem [53–56]. So far however, these lasers seem to be rather delicate to handle. An interesting alternative are lasers that avoid the use of microstructure fibers in another way.

Yet another class of frequency combs that can stay in lock for even longer times are fs fiber lasers [59]. The most common type is the erbium doped fiber laser that emits within the telecom band around 1500 nm. For this reason advanced and cheap optical components are available to build such a laser. The mode locking mechanism is similar to the Kerr lens method, except that non-linear polarization rotation is used to favor the pulsed high peak intensity operation. Up to a short free space section that can be build very stable, these lasers have no adjustable parts. Bulk fused silica has its zero group velocity dispersion at around 1.2 μm but this can be shifted to 1.5 μm in an optical fiber. If in addition the radial dependence of the refractive index is designed to obtain a small core area A_f, the fiber becomes what is called a highly non-linear fiber (HNLF) without any microstructure. These HNLF's are commercially available and can be spliced directly to a fs fiber laser. This virtually eliminates the remaining alignment sensitive parts as the free space frequency doubling stage and beat note detection can be build rather robust. Continuous stabilized operation for many hours [60, 61] have been reported. The Max-Planck Institute für Quantenoptik in Garching (Germany) operates a fiber based self referenced frequency comb that stays locked without interruption for months.

C. Self-referencing

The measurement of ω_{CE} fixes the position of the whole frequency comb and is called self-referencing. The method relies on measuring the frequency gap between *different* harmonics derived from the *same* laser or frequency comb. The first crude demonstration [43] employed the 4th and the 3.5th harmonic of a $f = 88.4$ THz (3.39 μm) laser to determine ω_{CE} according to $4\omega_n - 3.5\omega_{n'} = (4n - 3.5n')\omega_r + 0.5\omega_{CE} = 0.5\omega_{CE}$ with $4n - 3.5n' = 0$. To achieve the condition of the latter equation both n and n' have to be active modes of the frequency comb. The required bandwidth is $0.5f = 44.2$ THz, which is what the 73 fs laser together with a single mode fiber as discussed in the previous chapter can generate.

A much simpler approach is to fix the absolute position of the frequency comb by measuring the gap between ω_n and ω_{2n} of modes taken directly from the frequency comb [10, 11, 47, 51]. In this case the carrier-envelope offset frequency ω_{CE} is directly produced by beating the frequency doubled (it should be noted that this does not simply mean the doubling of each individual mode, but the general sum frequencies generation of all modes. Otherwise the mode spacing, and therefore the repetition rate, would be doubled as well) red wing of the comb $2\omega_n$ with the blue side of the comb at ω_{2n}: $2\omega_n - \omega_{n'} = (2n - n')\omega_r + \omega_{CE} = \omega_{CE}$ where again the mode numbers n and n' are chosen such that $(2n - n') = 0$. This approach requires an octave spanning comb, i.e. a bandwidth of 375 THz if centered at the titanium-sapphire gain maximum at 800 nm.

Figure 12 sketches the $f - 2f$ self referencing method. The spectrum of a titanium-sapphire mode locked laser is first broadened to more than one optical octave with a microstructure fiber. A broad band $\lambda/2$ wave plate allows to choose the polarization with the most efficient spectral broadening. After the fiber a dichroic mirror separates the infrared ("red") part from the green ("blue"). The former is frequency doubled in a non-linear crystal and reunited with the green part to create a wealth of beat notes, all at ω_{CE}. These beat notes emerge as frequency difference between $2\omega_n - \omega_{2n}$ according to (4) for various values of n. The number of contributing modes is given by the phase matching bandwidth $\Delta\nu_{pm}$ of the doubling crystal and can easily exceed 1 THz. To bring all these beat notes at ω_{CE} in phase, so that they all add constructively an adjustable delay in form of a pair of glass wedges or corner cube is used. It is straight forward to show that the condition for a common phase of all these beat notes is that the green and the doubled infrared pulse reach the photo detector at the same time. The adjustable delay allows to compensate for different group delays, including the fiber. In practice the delay needs to be correct within $c\Delta\nu_{pm}$ which is 300 μm for $\Delta\nu_{pm}$=1 THz. Outside this range a beat note at ω_{CE} is usually not detectable.

A grating is used to prevent the extra optical power, that does not contribute to the signal but adds to the noise level, from reaching the detector. Typically only a large relative bandwidth of say 1 THz/375 THz needs to be selected so that a very moderate resolution illuminating 375 lines is sufficient. For this reason it is usually not necessary to use a slit between the grating and the photo detector. Sufficient resolution can be reached with a small low cost 1200 lines per mm grating illuminated with a beam collimated with $\times$10 microscope objective out of the microstructured

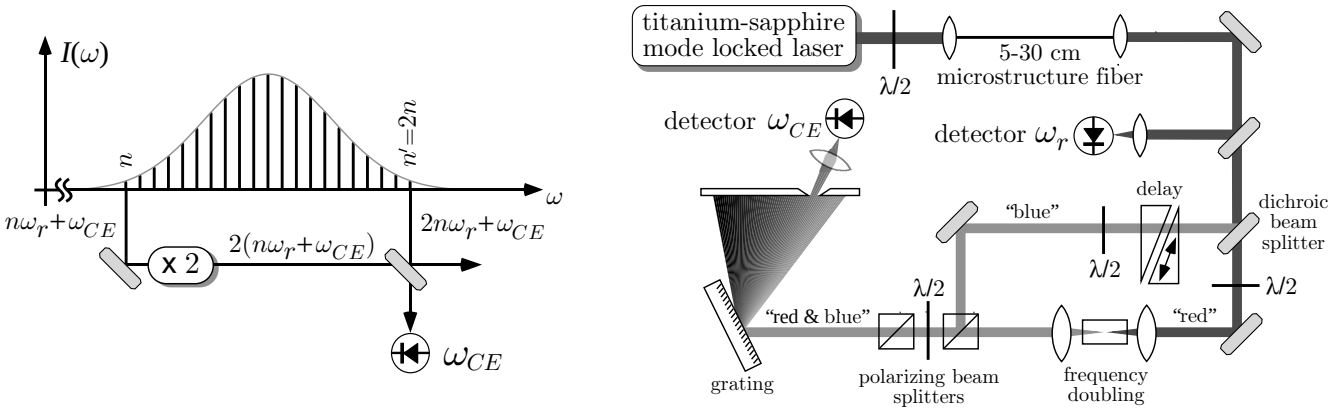

FIG. 12: *(left) — The principle of $f-2f$ self referencing by detecting a beat note at ω_{CE} between the frequency doubled "red" wing $2(n\omega_r+\omega_{CE})$ of the frequency comb and the "blue" modes at $2n\omega_r+\omega_{CE}$. (right) — More detailed layout of the self referencing scheme. See text for details.*

fiber.

When detecting the beat note as described above, more than one frequency component is obtained for two reasons. First of all any beat note, even between two cw lasers, generates a two components because the radio frequency domain can not decide which of the two optical frequencies is larger than the other. Secondly, observing the beat notes between frequency combs, not only the desired component $k=2n-n'=0$ is registered, but all integer values of k, positive and negative contribute, up to the bandwidth of the photo detector. This leads to a set of radio frequency beat notes at $k\omega_r \pm \omega_{CE}$ for $k=\ldots-1,0,+1\ldots$. In addition the repetition rate, including its harmonics will most likely give the strongest components. After carefully adjusting the nonlinear interferometer, spatially and spectrally, and scanning the delay line for the proper pulse arrival times, the radio frequency spectrum may look like the one shown in Fig. 13. A low pass filter with a cut-off frequency of $0.5\omega_r$ selects exactly one beat note at $\pm\omega_{CE}$. The design of such a filter may be tricky, mostly depending on how much stronger the repetition rate signal exceeds the beat note at ω_{CE}. The sketch in Fig. 13 gives a feeling on how steep this filter needs to be at the cut-off in order to suppress the unwanted components below the noise level. Such a suppression is required for taking the full advantage of the signal to noise ratio. For this reason it is desirable to work at higher repetition rates. At ω_r around $2\pi\times 800$ MHz, as used mostly with ring titanium-sapphire lasers, the filter requirements are much more relaxed than say at 80 MHz. In addition, a larger repetition rate concentrates more power in each mode further improving the beat notes with the frequency comb.

As described, both degrees of freedom ω_r and ω_{CE} of the frequency comb can be measured up to a sign in ω_{CE} that will be discussed below. For stabilization of these frequencies, say relative to a radio frequency reference, it is necessary to be able to control them. Again the repetition rate turns out to be simpler. By mounting one of the lasers cavity mirrors on a piezo electric transducer allows to control the pulse round trip time. Another option is offered by

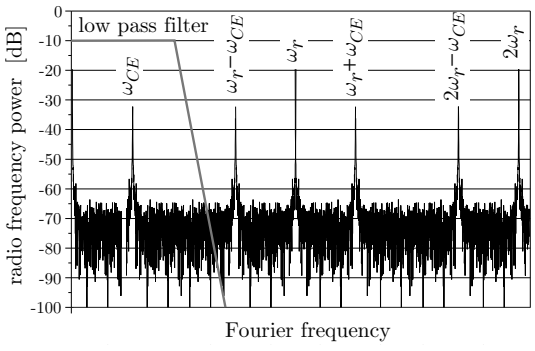

FIG. 13: *Radio frequency spectrum produced by a self referencing non-linear interferometer such as the $f-2f$ interferometer shown in Fig. 12. A low pass filter with a cut-off at $0.5\omega_r$ selects the component at $\pm\omega_{CE}$.*

mode locked lasers that use prism pairs to compensate the intracavity group velocity dispersion. In this case tipping the mirror at the dispersive end where the cavity modes are spatially separated, changes the relative cavity lengths of the individual modes and thereby the mode spacing in frequency space [10]. In practice the detected repetition frequency is mixed with the radio frequency reference, i.e. the frequency difference is generated, lowpass filtered and with appropriate gain send back to the piezo electric transducer. When properly designed such a phase locked loop forces one oscillator, the repetition rate, to stay in phase with another, the radio frequency reference.

Setting up a phase locked loop for the repetition rate therefore seems rather straightforward. However, some caution concerning the servo bandwidth needs to be observed. It turns out that the large frequency multiplication factor n in (4) may also multiplies the noise of the reference oscillator. The phase noise power for direct frequency multiplication by n increases proportional to n^2 [63], so that a factor of $n = 10^6$, that would take us from a 100 MHz radio frequency signal to a 100 THz optical signal, increases the noise by 120 dB. On this basis it has been predicted that, using even the best available reference oscillator, it is impossible to multiply in a single step from the radio frequency domain into the optical [25]. The frequency comb does just that but avoids the predicted carrier collapse. In this case the laser acts as a flywheel in the optical that does not follow the fast phase fluctuations of the reference oscillator but averages them out. In this sense the n^2 multiplication law does not apply, because it assumes a phase stiff frequency multiplication that would correspond to an infinite servo bandwidth. Fortunately a typical free running titanium-sapphire mode locked laser shows very good phase stability of the pulse train on its own. For averaging times shorter than typical acoustic vibrations of several ms period, such a laser shows better phase stability than a high quality synthesizer. It is therefore essential to use a moderate servo bandwidth for phase locking the repetition rate of a few 100 Hz at most. A small servo bandwidth may be implemented electronically by appropriate filtering or mechanically by using larger masses than the usual tiny mirrors mounted on piezo transducers for high servo speed. In some case a complete one inch mirror mount has been moved for controlling the repetition rate [64].

Controlling the carrier envelope frequency requires some effort. Experimentally it turned out that the energy of the pulse stored inside the mode locked laser has a strong influence on ω_{CE}. After initial explanations of this effects turned out to be too crude, more appropriate mechanisms have been found [65]. Conventional soliton theory [66] predicts a dependence of the phase velocity but no dependence of the group velocity on the pulse peak intensity. Any difference in the cavity round trip phase delay and the cavity round trip group delay results in a pulse to pulse carrier envelope phase shift and therefore a non-vanishing ω_{CE}. However, the intensity dependence of that effect may turn out to have the wrong sign [67]. The reason is that higher order effects, usually neglected in the conventional soliton theory, play an important role.

To phase lock the carrier envelope offset frequency ω_{CE}, one uses an actuator, in most cases an acousto-optic modulator, that drains an adjustable part of the pump laser power. Electro-optic modulators have also been used, but they have the disadvantage that they need to a bias voltage that wastes some of the pump energy to work in the linear regime. To servo control the phase of the ω_{CE} component usually requires much more servo bandwidth than locking the repetition rate. How much is needed in practice depends on the type of laser, the intensity and beam pointing stability of the pump laser and the phase detector in use.

In most cases a simple mixer is not sufficient to unambiguously detect the phase of ω_{CE} relative to a reference oscillator as the expected in-loop phase fluctuations are usually much larger as for the ω_r servo. Prescalers or forward-backward counting digital phase detectors may be used to allow for larger phase fluctuations, that in turn allow the use of moderate speed (several 10 kHz) electronics. A complete circuit that has been used for that purpose very successfully is published in [68]. Stabilizing the carrier envelope frequency, even though it generally requires faster electronics, does not have the stability and accuracy issues that enter via the repetition rate due to the large factor n in (4). Any fluctuation or inaccuracy in ω_{CE} just adds to the optical frequencies rather than for ω_r in the radio frequency domain where it is subsequently multiplied by n.

Finally it should be mentioned that none of the controls discussed here acts solely on either frequency ω_{CE} and ω_r. In general a linear combinations of the two is affected. In practice this turns out to be not important because the different speeds of the two servo systems ensure that they don't influence each other.

D. Measurement of the $1S-2S$ frequency in atomic hydrogen

Measuring the frequency of the dye laser used for hydrogen $1S-2S$ spectroscopy at ω_L with a stabilized frequency comb, involves the creation of yet another beat note ω_b with the comb (see Fig. 7). For this purpose the beam of the cw laser is matched with the beam that contains the frequency comb, say with similar optics components as used for creating the carrier envelope beat note. A dichroic beam splitter, just before the grating in Fig. 12, could be used to reflect out the spectral region of the frequency comb around ω_L without affecting the beat note at ω_{CE}. This beam would then be fed into another set-up consisting of two polarizing beam splitters, one half wave plate, a grating and

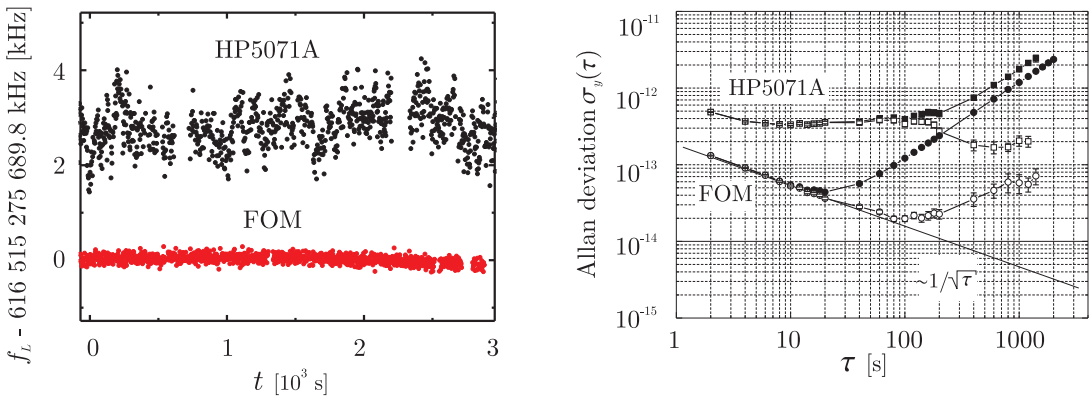

FIG. 14: *(left) — Two different samples of the optical frequency $f_L = \omega_l/2\pi$ of the 486 nm dye laser locked to a reference cavity with the self-referenced $f-2f$ frequency comb. As a radio frequency reference we used either the transportable fountain clock FOM from BNM-SYRTE Paris or a commercial Cs atomic clock (Agilent model HP5071A). A linear drift is removed from the displayed data. (right) — Allan deviation for the data shown at the left part of the figure. Solid squares and circles represent raw data, while the hollow symbols correspond to data with subtracted linear drift.*

a photo detector for an optimum signal to noise ratio. The frequency of the cw laser is then given by

$$\omega_L = n\omega_r \pm \omega_{CE} \pm \omega_b \tag{13}$$

where the same considerations as above apply for the sign of the beat note ω_b. These signs may be determined by subsequently introducing small changes to ω_r and ω_{CE} and observing the corresponding shift in ω_b. This uniquely fixes both signs if ω_L is held fixed during this test.

The last quantity that needs to be determined is the mode number n. If the optical frequency ω_L is already known to a precision better than the mode spacing, the mode number can simply be determined by solving the corresponding equation (13) for n and picking the nearest integer. For hydrogen this poses no difficulty since the $1S-2S$ transition frequency has been known for decades with a much better accuracy than the 800 MHz mode spacing used here. Therefore determining n from the previous result should yield a value n very close to integer. If this method fails a coarse measurement could be provided by a wave meter for example if its resolution and accuracy is trusted to be better than the mode spacing of the frequency comb. In our 2003 hydrogen measurement for example we determined $n = 770\,644$ for a chosen $\omega_r = 2\pi \times 800\,\mathrm{MHz}$ and $\omega_{CE} = 2\pi \times 40\,\mathrm{MHz}$. The beat frequency ω_b then turs out to be around 35.7 MHz with the laser tuned close to the $F = 1 \rightarrow F = 1$ hyperfine component of the $1S-2S$ transition.

For both the 1999 and 2003 measurements, a transportable Cs fountain clock (FOM) from BNM-SYRTE (now called LNM-SYRTE) Paris [69] has been installed at MPQ, Garching. This clock operates with an Allan deviation of $1.8 \times 10^{-13}\tau^{-1/2}$, where τ measures the averaging time in seconds. Its accuracy has been evaluated to 8×10^{-16} [70], but during the experiments in Garching, a verification only at the level of 2×10^{-15} has been performed which is still one order of magnitude better than required for the $1S-2S$ transition.

A series of measurements with the 486 nm dye laser locked to the horizontal reference cavity is shown in Fig. 14. For comparison we show data obtained with a commercial Cs atomic clock (Agilent model HP5071A) and the fountain clock. The superior short term stability of the latter can be seen immediately from these data. In addition a rapid variation due to the Cs clock and the long term drift of the reference cavity can be distinguished and subtracted from the data. To further average the short term stable reference cavity with the absolute accuracy of the Cs clock we fit parabolas to 500 s intervals of the reference cavity frequency data. This choice has been made by observing the Allan variance of the Cs clock in comparison with the Allan variance of the reference cavity (see Fig. 14 (right)). The averaging procedure uses time tags recorded with each data point, that also contain the Lyman-α count rate. The fitted parabola then determines the average cavity frequency as a function of time within the 500 s interval. For the data analysis the parabolas are used instead of the direct measurements of ω_L, knowing the AOM detuning between the laser and the reference cavity (see Fig. 7).

The hydrogen $1S-2S$ florescence data analyzed in this way has been obtained during 10 days in 1999 [71] and 12 days in 2003 [9]. For comparability, both data sets have been analyzed using the same theoretical line-shape model [4] (see Fig. 8 (left)). The line centers obtained from one day of data collection are presented in Fig. 15 (left) as an example. Plotted as a function of laser power the ac Stark shift becomes clearly visible. To remove this systematic shift we fit a linear function and extrapolate to zero power. The same procedure is repeated for every data

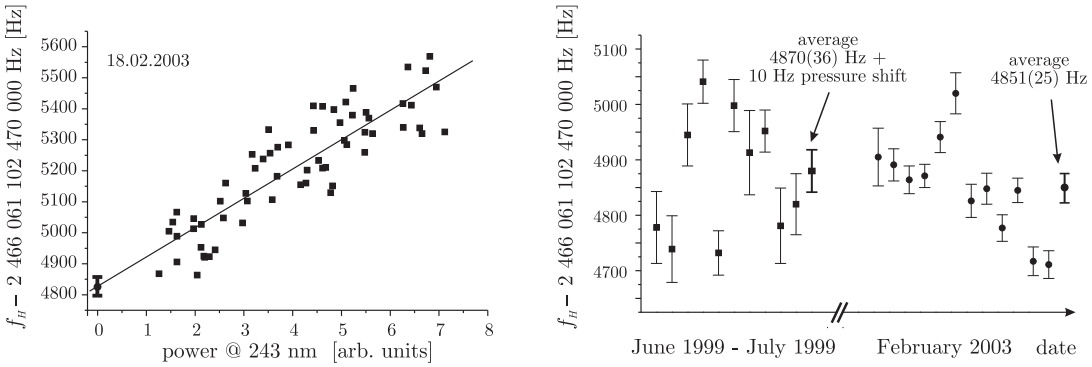

FIG. 15: *(left) — Line centers found from the measurement of the* $1S-2S$ *absolute frequency during one day as a function of laser power to determine the ac Stark shift. Using a linear fit we derive the transition frequency at zero excitation intensity. (right) — Result of 10 days of measurement in 1999 and 12 days in 2003. The error bars represent statistical uncertainty for each day only. The 1999 and 2003 averaged results are calculated without weighting with these error bars. According to this data an upper limit on the drift rate of the hydrogen* $1S-2S$ *absolute frequency of* $(-3.2 \pm 6.3) \times 10^{-15}$ *yr*$^{-1}$ *may be derived.*

taking day to obtain the complete data set shown at right hand side of Fig. 15. The error bars are calculated as the standard deviations of the mean values and do represent the respective statistical uncertainty only. In comparison this uncertainty was significantly reduced for the 2003 data set due to a narrower laser line width and a better signal-to-noise ratio. However, the variance of the day averages did not reduce accordingly in order to have roughly 2/3 of the error bars overlapping as required for good statistics. We conclude that an uncompensated varying systematic shift has entered the data. We believe to have identified two contributions caused by deviations of the laser and the atomic beam from cylindrical symmetry. This may give rise to a residual first-order Doppler shift. Later measurements performed without the fountain clock with a deliberately introduced asymmetry in the 243 nm cavity indicate an adjustment-dependent frequency shift. In addition having the atomic and the laser beam not exactly centered on axis may influence the laser power calibration, because the latter detects a value integrated over the transverse dimension of the enhancement cavity mode whereas the atoms may sample the laser field with a different weight according to their spatial distribution. These effects should average out after multiple re-adjustments of the spectrometer, which has been performed typically twice a day. Unfortunately it is impossible to correct the data *a posteriori* because such details of the spectrometer adjustment were not recorded during the measurement. Other effects which can cause a systematic shift (intra-beam pressure shift, background gas pressure shift, Stark shift of the hyperfine levels induced by the rf gas discharge, stray electric fields) have been checked and can be excluded on the level of the observed day to day variance.

Because of these problems with the statistical error bars, the 1999 and 2003 day-dependent data were averaged without using them as a weight. The 2003 average value for the $F = 1$, $m_F = \pm 1 \rightarrow F' = 1$, $m'_F = \pm 1$ component

Contribution	$f_{\mathrm{H},1999}$ [Hz]	$\sigma_{\mathrm{H},1999}$ [Hz]	$f_{\mathrm{H},2003}$ [Hz]	$\sigma_{\mathrm{H},2003}$ [Hz]
Extrapolated value − 2 466 061 102 474 kHz	870	36	851	25
Background gas pressure shift	10	10	0	2
Intra-beam pressure shift	0	10	0	10
Line shape model	0	20	0	20
DC Stark shift	0	5	0	5
Blackbody radiation	0	1	0	1
Standing wave effects	0	10	0	1
Intensity zero uncertainty	0	1	0	0
Fountain clock uncertainty	0	5	0	5
Total − 2 466 061 102 474 kHz	880	45	851	34

TABLE I: Results of the ($1S$, $F = 1$, $m_F = \pm 1 \rightarrow 2S$, $F' = 1$, $m'_F = \pm 1$) transition frequency measurement ($f_{\mathrm{H},1999}$, $f_{\mathrm{H},2003}$) and uncertainty budgets ($\sigma_{\mathrm{H},1999}$, $\sigma_{\mathrm{H},2003}$) for the 1999 and 2003 measurements correspondingly.

of the hydrogen $1S-2S$ transition is determined as

$$f_{\mathrm{H}} = 2\,466\,061\,102\,474\,851\,(34)\,\mathrm{Hz} \tag{14}$$

This result along with the 1999 value and the main statistical and systematic uncertainties are summarized in Table I. It should be noted that the 2003 measurement did not yield a significant reduction of the overall uncertainty. The two results are in agreement within their mutual uncertainties and can be used as an upper limit on a possible slow variation of that transition frequency. We obtain an upper limit of the difference of (-29 ± 57) Hz between the measurements that are 44 months apart. This is equivalent to a fractional time variation of the ratio $f_{\mathrm{H}}/f_{\mathrm{Cs}}$ equal to $(-3.2 \pm 6.3) \times 10^{-15}$ yr^{-1}, where the ground state hyperfine splitting of ^{133}Cs, which is used as a reference in these measurements, is given by f_{Cs}. We will use this result for further analysis in Section V.

IV. DETERMINATION OF FUNDAMENTAL ATOMIC PARAMETERS

During the last decades, a number of high-precision experiments employing two-photon spectroscopy of the $1S-2S$ transition in atomic hydrogen and deuterium have been performed. These measurements have been motivated by the possibility to check highly accurate QED calculations and to derive atomic parameters such as the Rydberg constant R_∞. In this section we briefly present the analysis of the world hydrogen data for that purpose and a recent measurements of the $2S$ hyperfine structure.

A. The Rydberg constant and the Lamb shift

The hydrogen atom offers the best opportunity to precisely determine the Rydberg constant R_∞ which scales all atomic energy levels. Since it is made up of other fundamental constants, it can be used as a corner stone to adjust the set of all fundamental constants such that their recommended values are in best agreement with existing experimental data [72]. Strictly speaking the Rydberg constant scales only the Dirac energies correctly. Recoil corrections and higher order terms, known as the Lamb shift, scale with powers of the fine structure constant and the electron to proton mass ratio. The latter can be determined with very high accuracy by storing electrons and protons in a Penning trap and compare their cyclotron frequencies [73]. Therefore at least two different hydrogen frequency measurements are required to determine the remaining two parameters. One common way to analyze the world hydrogen data is to express the experimental data in terms of the Rydberg constant and the Lamb shifts of the involved levels. The Lamb shift values are than interpreted as a test of QED.

Extended reviews of radio frequency and optical measurements of different transitions in atomic hydrogen are presented in [2, 74]. Besides the precise determination of the absolute frequencies of the $1S-2S$ and the $2S-nS, D$ (with $n = 8, 10, 12$) transitions, radio frequency data of adjacent S and P levels [75] as well as combinations of optical frequencies enter this analysis. The latter method exploits the crude scaling of hydrogen energy levels with the inverse principal quantum number n squared. This allows to excite optical transitions with almost integer ratios of frequencies that can be readily related by frequency doubling of some of the involved lasers. The recorded frequency differences are direct measurements of the deviations from the Bohr energy levels and therefore allow the extraction of the Lamb shifts in a simple way. Frequency combinations of this type have been measured at the *Laboratoire Kastler Brossel, Paris* by comparing the $2S-6S$ frequency with one quarter of the $1S-3S, D$ frequencies. Along the same line the frequencies of the $2S-4S, P, D$ have been compared with one quarter of the $1S-2S$ frequency at Garching [77] and Yale [76]. In addition the analysis of the hydrogen world data uses the approximate $1/n^3$ scaling for the Lamb shifts, which allows the accurate calculation of the Lamb shift differences $L(1S) - n^3 L(nS)$. Combinations of all this data, including related measurements in deuterium, allows for a least square adjustment using the quantities of interest as a parameter. These quantities are the $1S$ Lamb shift $L(1S) = 8\,172.840(22)$ MHz and the Rydberg constant $R_\infty = 109\,737.315\,685\,50(84)\,\mathrm{cm}^{-1}$ as derived in the described way in [2]. Because of the $1/n^3$ scaling law for the Lamb shifts, its $1S$ value is the largest and provides the largest lever when confronting it with theoretical QED results.

In comparison the result for the Rydberg constant from the hydrogen least squares adjustment agrees well with the 2002 CODATA recommended value $R_\infty = 109\,737.315\,685\,25(73)\,\mathrm{cm}^{-1}$ [79]. This is no surprise as this estimation draws on mostly the same input data. With its relative uncertainty of 6.6×10^{-12} the Rydberg constant is the most accurately known fundamental constant.

To compare the result of the least squares adjustment for the $1S$ Lamb shift with a relative uncertainty of 2.7×10^{-6} to QED predictions one faces the problem that the proton charge radius, that enters the theory, is not known with sufficient accuracy. Even though this proton size correction is a small contribution to the $1S$ Lamb shift, it has

the largest contribution to its uncertainty. In part this is also due to the variety of disagreeing values found in the literature. This least squares experimental value is in a good agreement with theoretical predictions, if one assumes the Mainz value for the proton charge radius of $r_p = 0.862(12)$ fm [80] and includes results of QED two-loop contributions given in [81].

For further improvements it should be noted that the $1S-2S$ transition frequency is known with by far the highest accuracy. Because at least two parameters have to be determined from the hydrogen world data as explained above, the second best measurement determines the uncertainty of all results. It is therefore advisable to try to improve other transition frequencies besides the $1S-2S$ in atomic hydrogen. One of the possibilities would be to determine a value of the $1S-3S$ frequency [82]. An experiment on measuring the $1S-3S$ two-photon transition frequency in a cold atomic beam by excitation with ps pulse train is also planned in Garching [83]. There is also an on-going activity on improving the proton charge radius by performing spectroscopy in muonic hydrogen at the Paul Scherrer Institute [84] and $1S-2S$ in He^+ at Garching [85] which can further improve values of the Rydberg constant and the Lamb shift.

B. The $2S$ hyperfine structure

The frequencies of the $2S$ hyperfine intervals $f_{\rm HFS}(2S)$ in atomic hydrogen and deuterium have been measured several times during 20th century by driving the magnetic-dipole transition in an atomic thermal beam [86–88]. The relative accuracy of these measurements (150-300 ppb) exceeds the accuracy of the theoretical prediction which is restricted by insufficient knowledge of the proton structure. However, very similar to the related problem for the Lamb shifts, a specific combination of hyperfine splittings can be calculated with much higher precision. For the $1S$ and $2S$ hyperfine intervals this combination reads

$$D_{21} = 8f_{\rm HFS}(2S) - f_{\rm HFS}(1S) \tag{15}$$

and can be calculated without detailed knowledge of the nuclear structure effects (see [8] and references therein). Again this results from the fact, that energy correction due to a finite size of nucleus scales as $\Delta E_{\rm nucl} \sim 1/n^3$ and significantly cancels in D_{21}. The $1S$ hyperfine splitting in hydrogen is one of the best known transition frequencies and does not pose a limit to the accuracy of (15). By adding an experimental value for the $2S$ hyperfine interval $f_{\rm HFS}(2S)$ the resulting value for D_{21} can be compared with the QED value. This QED test is currently limited by the experimental uncertainty for $f_{\rm HFS}(2S)$.

For this reason we have decided to use our spectrometer for a new measurement of the $2S$ hyperfine interval in atomic hydrogen and deuterium. The experimental setup is very similar to the one depicted in Fig. 7 except that for this measurement a two layer magnetic shielding has been added to suppress the ambient field to below 1 mG. At this low magnetic field the frequency of the $2S$ hyperfine splitting $f_{\rm HFS}(2S)$ can be expressed through

$$f_{\rm HFS}(2S) = f_{\rm HFS}(1S) + f(\beta) - f(\alpha)\,, \tag{16}$$

where $f(\beta)$ and $f(\alpha)$ are frequencies of corresponding two-photon transitions that are shown in Fig. 16. Since the ground-state hyperfine splitting $f_{\rm HFS}(1S)$ is known to a very high accuracy, both for hydrogen and deuterium, it

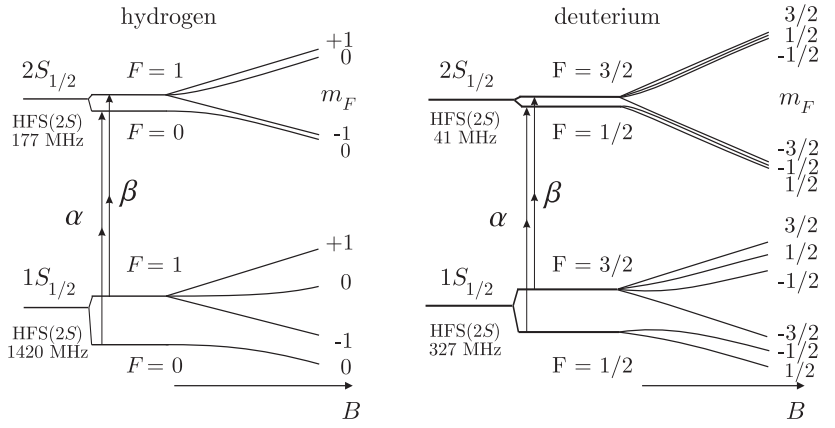

FIG. 16: *Hyperfine and Zeeman sublevels of the $1S$ and $2S$ states in hydrogen (left) and deuterium (right) and shifts cause by a magnetic field B.*

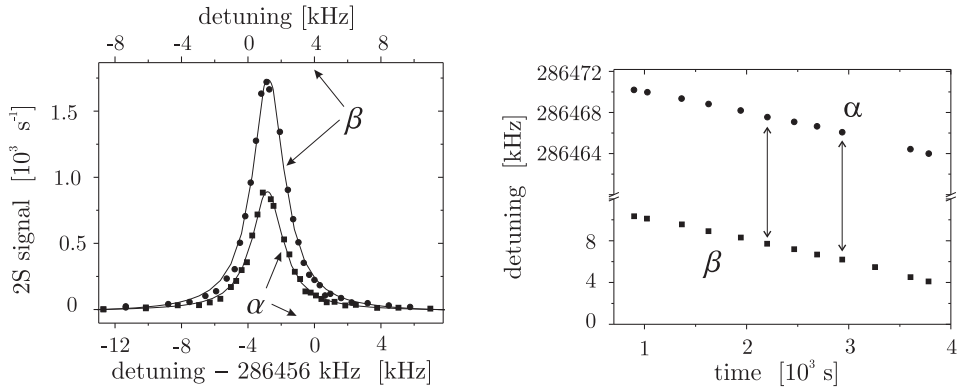

FIG. 17: *(left) — Nearly simultaneous detection of two-photon hyperfine transitions α and β in atomic deuterium. Lines recorded with a delay $\Delta\tau = 610\,\mu$s and Lorentzian fits are presented. (right) — Evaluation of the difference $f(\alpha) - f(\beta)$. The data is fitted with a pair of parallel lines so that the slope and the frequency difference can be determined.*

is enough to determine the frequency difference $f(\beta) - f(\alpha)$. This difference is in the radio frequency region, so that no absolute optical frequency measurement is required. The measurement has been performed by recording the components $f(\beta)$ and $f(\alpha)$ in short sequence using the horizontal reference cavity sketched in Fig. 1 as a flywheel. The AOM shifter shown Fig. 7 allows us to change quickly between the hyperfine components.

For the measurement in hydrogen we have recorded spectral lines of transitions α and β in time intervals of a few minutes. For measurements in deuterium we have recorded lines nearly simultaneously by alternating between the hyperfine components for individual one second gate time data points [6]. The result of such a simultaneous scan is shown on the left hand side of Fig. 17. We only account for Lyman-α photons with a delay of $\Delta\tau = 610\,\mu$s as explained in Section II B by fitting them with Lorentzians. After that we plot the frequencies of line centers against time for both transitions α and β and determine the frequency difference by subtracting the cavity drift as shown on the right hand side of Fig. 17. For this differential measurement, the most significant systematic effects of two-photon beam spectroscopy cancel out. As shown in [5], the differential dynamic Stark is rejected by common mode at a level of 10^{-6} relative to the shift of the $1S-2S$ transition (the latter being around 500 Hz). The second order Doppler effect and line asymmetries cancel very effectively as well. The residual dc Stark shift and the magnetic fields contribute at a level of a few hertz. The upper limit of the pressure shift has been determined experimentally by changing the atomic flux.

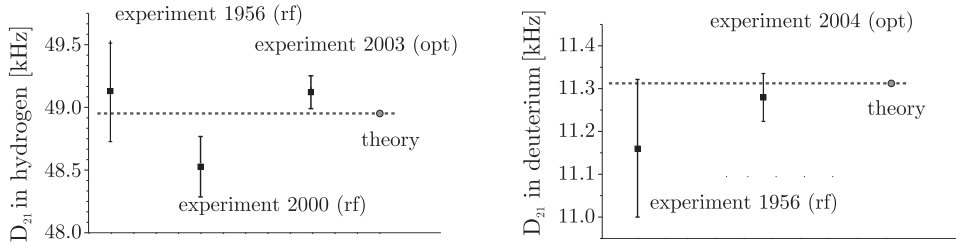

FIG. 18: *Specific frequency difference D_{21} in atomic hydrogen (left) and deuterium (right). Experimental [5, 6, 86–88] and theoretical values [8] along with their uncertainties are presented.*

Using our spectrometer the hyperfine splitting of the $2S$ level in atomic hydrogen and deuterium has been determined to $f^{(\mathrm{H})}_{\mathrm{HFS}}(2S) = 177\,556\,860(16)$ Hz [5] and $f^{(\mathrm{D})}_{\mathrm{HFS}}(2S) = 40\,924\,454(7)$ Hz [6]. With this the optical measurement became several times more accurate than the traditional radio frequency method. The resulting D_{21} specific frequency differences are in a good agreement with theoretical predictions [8] as shown in Fig. 18. These tests allow to selectively verify higher-order QED contributions beyond the $1/n^3$ scaling law with a sensitivity approaching QED tests in leptonic systems (like ground-state HFS study in muonium [7]) which are virtually free from hadronic contributions.

V. CONSTANCY OF THE FINE STRUCTURE CONSTANT AND OPTICAL CLOCKS

The question of constancy of fundamental constants was first raised in Dirac's "large number hypothesis" (1937) which aimed for a harmonization of the basic laws of physics [89]. Since then, this hypothesis has been reviewed and extended by many other scientists opening a broad field of theoretical and experimental investigations. As there is no accepted theory predicting the values of fundamental constants, the question of their possible time variation belongs mostly to the field of experimental physics. In the last decades a number of different astrophysical, geological, and laboratory methods have been used to search for their possible variation in different time epochs with an ever increasing sensitivity (for details see the review [90]). From the point of view of its importance for physics in general, these investigations are at the same level as tests of CPT-symmetry and the search for an electric dipole moment of elementary particles.

The basic principle of every experimental search for a time variation of fundamental constants is the measurement of a physical quantity $\Phi(\gamma_1, \cdots, \gamma_K, t)$, which is a function of several fundamental constants γ_i, at times t_1 and t_2, separated by the interval $\Delta t = t_1 - t_2$. If $\Phi(\gamma_1, \cdots, \gamma_K, t)$ is a function of more than one constant ($K > 1$) it is not possible to derive separate values for $\Delta\gamma_i$ even if the dependence of Φ on γ_i is straightforward. However, repeated measurements on several physical quantities Φ_j with $j = 1, \cdots, N$ and ($N \geq K$) or assumptions on restrictions or mutual correlations of the constants of their drifts may be used to derive all $\Delta\gamma_i$ involved. Lacking any accepted theory of the variation of fundamental constants one ideally prefers to draw conclusions with the smallest set of assumptions.

Concerning the time interval Δt, there are two extreme classes of experiments: (i) astronomical or geological observations (e.g. of quasar spectra and the Oklo phenomenon [91]) and (ii) high precision laboratory frequency comparisons of atomic, molecular or ionic transitions. The investigation of absorption or emission lines of distant galaxies back illuminated by the white light of quasars at even larger distances takes advantage of the extremely long look back time up to 10^{10} years. In contrast to that, laboratory frequency comparisons are restricted to short time intervals of a few years but win considerably in relative sensitivity, which can be of the order of 10^{-15} or better. As a result the sensitivity in terms of relative variation per year can be comparable for both classes of experiments. Important advantages of laboratory experiments in general are: The variety of different systems that may be tested, the possibility to change parameters of the experiments in order to control systematic effects and the straightforward determination of the drift rates from the measured data. Modern metrology precision frequency measurements deliver information about the stability of the to-date values of the constants, which can only be tested with laboratory measurements. At the same time only non-laboratory methods are sensitive to processes that happened in the early universe, which can be much more severe as compared to the present time. As both classes of experiments (i), (ii) probe $\Delta\gamma_i$ at different epochs, they supplement each other to get a more detailed view of the possible time variation of fundamental constants.

A. Astrophysical and geological methods: a brief review

Due to the large look back time the sensitivity of astrophysical and geological methods to monotonic long-time drifts is very high. A recent analysis of quasar absorptions of redshifted UV transition lines [92] indicates a variation of α at the level of $\Delta\alpha/\alpha = (-0.54 \pm 0.12) \times 10^{-5}$ in the first half of the evolution of the universe (5–11 Gyr ago) [92, 93]. There are also indications that during this period, the electron to proton mass ratio was different from its current value on the same level of 10^{-5} [94, 95]. The analysis of astrophysical data requires a number of model assumptions which include not only the well-established scenarios of the evolution of the universe, but also assumptions about isotope abundances in interstellar gas clouds, the presence of magnetic fields and others (see the review [90]) which are difficult to verify. More recent observations of quasar absorption spectra [96, 97], performed by different groups, seem to rule out a variation of α at this level but their data has very recently been partially re-analyzed leading to different conclusions [98].

A very stringent limit for the time variation of α on geological time scales derives from the analysis of isotope abundance ratios in the natural fission reactor of Oklo, Gabon, which operated about 2 Gyr ago. A recent re-analysis of the $^{149}\mathrm{Sm}/^{147}\mathrm{Sm}$ isotope abundance ratio sets a limit of $\Delta\alpha/\alpha = (-0.36 \pm 1.44) \times 10^{-8}$ [91]. There were attempts to use a model of a "damped oscillator" [99] to fit both Oklo data [91] and results derived form quasar absorption spectra [92, 93]. The interpretation of the Oklo data is not unambiguous, as the result strongly depends on reactor operating conditions which are not exactly known. Selecting another possible reaction branch yields a value of $\Delta\alpha/\alpha = (9.8 \pm 0.8) \times 10^{-8}$ [91]. In contrast to the first one, this result indicates a non-zero drift.

B. High-precision laboratory measurements and variation of the fine structure constant

So far all laboratory measurement of the drift rates of fundamental constants are based on comparisons of electromagnetic transitions that depend in a different way on these constants. The non-relativistic scalings of gross-, fine- and hyperfine transitions in atoms, ions and molecules are summarized in Table II. In contrast to the previous Sections on high precision measurements a first order theory is sufficient here, as none of the drifts have been detected yet with small relative uncertainty. To evaluate the possible drift of α one measures a frequency ratio of two transitions of different types, for example a gross structure and a fine structure component. Pioneering astrophysical measurements of the α drift [100, 101] used exactly this method which is now called the "alkali-doublet method".

Sample	Transition	Scaling factor
Atom, ion		
	gross structure	Ry
	fine structure	$\alpha^2 Ry$
	hyperfine structure	$g_{\rm nucl}(\mu_N/\mu_B)\alpha^2 Ry$
Molecule		
	gross structure	Ry
	vibration structure	$(m_e/m_p)^{1/2} Ry$
	rotatoinal structure	$(m_e/m_p) Ry$

TABLE II: Scaling factors for different atomic systems in non-relativistic approximation. Here Ry is the Rydberg constant in hertz, $g_{\rm nucl}$ is the nuclear g-factor, μ_N and μ_B – nuclear and Bohr magnetons respectively, m_e and m_p – electron and proton mass respectively. In the relativistic case, i.e. for heavier atoms, it is necessary to multiply the scalings with relativistic correction $F_{\rm rel}(Z\alpha)$ that depends only on the fine structure constant and may be determined from relativistic Hartree-Fock calculations.

In the first laboratory measurements of α, the stability of frequency ratios between two hyperfine transitions in the radio frequency domain have been studied (see [102–104]). Ground-state hyperfine transitions in atoms and ions have very high Q-factors and allow a high sensitivity of these measurements. In the non-relativistic approach α should cancel according to the scaling given in Table II. However, in a real situation the values in that table need to be multiplied with a relativistic correction $F_{\rm rel}(Z\alpha)$ that depends only on the fine structure constant and may be determined from relativistic Hartree-Fock calculations. Taking this into account the ratio of hyperfine transition frequencies do indeed show a dependence on α so that it becomes possible to evaluate $\dot\alpha$ from such a comparison. For alkali atoms there exists an approximate expression for the relativistic correction called the Casimir correction [105] which reads as

$$F_{\rm rel}(Z\alpha) = \frac{3}{\lambda(4\lambda^2-1)}\,, \qquad \text{where} \qquad \lambda \equiv \sqrt{1-(Z\alpha)^2}\,. \tag{17}$$

For heavy atomic systems $F_{\rm rel}(Z\alpha)$ significantly differs from 1 (e.g. $F_{\rm rel}$=1.39 for Cs) and possesses high sensitivity for α variations:

$$L_\alpha^{\rm (HFS)} \equiv \alpha\frac{\partial}{\partial\alpha}\ln[F_{\rm rel}(Z\alpha)] = (Z\alpha)^2\frac{12\lambda^2-1}{\lambda^2(4\lambda^2-1)}\,. \tag{18}$$

A more exact calculation of the relativistic corrections will result in insignificant deviations from (18). For example, a more precise treatment of the relativistic correction to the Cs ground state hyperfine splitting yields $L_\alpha = 0.8$ [106] whereas the Casimir correction from (18) gives $L_\alpha = 0.74$. This small deviation does not significantly influence the accuracy of $\dot\alpha$ evaluations because it is mostly restricted by experimental uncertainties. One of the most sensitive tests of this type has been performed by A.Clairon's group at LNE-SYRTE, Paris where they compared frequencies of a Rb and a Cs atomic fountain clock [107]. This measurement resulted in $\partial/\partial t(\alpha^{-0.44} g_{\rm Rb}/g_{\rm Cs}) = (0.2 \pm 7.0)\times 10^{-16}\,{\rm yr}^{-1}$.

Unfortunately for optical transition frequencies $f^{\rm (opt)}$ no such approximation as the Casimir correction exists that would be useful for deriving the leading order dependence on the fine structure constant. For this reason relativistic Hartree-Fock calculations have been used. V. Dzuba *et al.* have expressed the results of their calculation in terms of two parameters q_1 and q_2 according to:

$$f^{\rm (HFS)} = f_0^{\rm (opt)} + q_1\left[\left(\frac{\alpha}{\alpha_0}\right)^2 - 1\right] + q_2\left[\left(\frac{\alpha}{\alpha_0}\right)^4 - 1\right]. \tag{19}$$

Z	Atom	Transition	λ [nm]	$L_\alpha^{(opt)}$
1	H	$1s\ S_{1/2}(F=1, m_F=\pm1) \rightarrow 2s\ S_{1/2}(F'=1, m'_F=\pm1)$	121	0
20	Ca	$^1S_0(m_J=0) \rightarrow {}^3P_1(m_J=0)$	657	0.03
49	In^+	$5s^2\ {}^1S_0 \rightarrow 5s5p\ {}^3P_0$	237	0.21
70	Yb^+	$6s\ {}^2S_{1/2}(F=0) \rightarrow 5d\ {}^2D_{3/2}(F=2)$	435	0.9
80	Hg^+	$5d^{10}6s\ {}^2S_{1/2}(F=0) \rightarrow 5d^96s^2\ {}^2D_{5/2}(F'=2, m'_F=0)$	282	−3.2

TABLE III: *Sensitivity of relativistic corrections $F_{\rm rel}(Z\alpha)$ to α for some atomic transitions according to [106, 108].*

Here $f_0^{(\rm opt)}$ and α_0 are the present day (or laboratory) values of the optical transition frequency and the fine structure constant respectively. This equation was used to describe quasar absorption spectra but may be used for laboratory measurements in which case $f_0^{(\rm opt)}$ and α_0 are also laboratory values but at different times. Results for the parameters q_1 and q_2 for various atoms and ions including some important optical clock transitions are published in [106, 108]. Only even powers in α enter the expansion (19) because the relativistic correction is proportional to $\sqrt{m_e^2+p^2}$, which contains even powers of electron momentum $p \sim Z\alpha$. Re-expressing V. Dzuba's notation in terms of the relativistic correction introduced above yields:

$$L_\alpha^{(\rm opt)} \equiv \alpha \frac{\partial}{\partial\alpha} \ln F_{\rm rel}(Z\alpha) = \frac{2q_1 + 4q_2}{f_0^{(\rm opt)}}\,. \tag{20}$$

Table III lists a few values of this quantity, that have been obtained in Refs. [106, 108] and are relevant for metrological transitions. Note, that for these calculations the value of Ry has been assumed to be fixed which imposes a constrain on the value of the product $m_e c^2\alpha^2/h$. However, another way of interpreting this is by picking Ry as the unit of frequency. Using the same units for all frequencies it will eventually drop out of all calculations and experimental data since in both cases, only frequency ratios are determined. This will become more clear from the analysis in the next Section.

Just as with the hyperfine structure, comparing optical transitions with different relativistic corrections becomes a powerful instrument to set an upper limit to the drift of fundamental constants. This method is widely used in astrophysical observations ("many-multiplet" method [92]) and in laboratory comparisons. An elegant realization of this method has been used by A. Cingöz *et al.* [109], by utilizing different relativistic corrections of two nearly degenerate levels of opposite-parity in neutral dysprosium. Monitoring the radio frequency transitions at 3.1 MHz for ^{163}Dy and 325 MHz for ^{162}Dy during 8 month only, the authors set a stringent limit on the drift of the fine-structure constant of $\partial\ln(\alpha)/\partial t = (-2.7 \pm 2.6)\times 10^{-15}\,\mathrm{yr}^{-1}$ without any assumptions about the drift of other constants. In the next Section we will describe how one can deduce a model-independent restriction to $\dot\alpha$ from different absolute optical frequency measurements.

C. Upper limit for the drift of the fine structure constant from optical frequency measurements

The determination of absolute optical frequencies means that these frequencies are measured in hertz, i.e. they are compared with the Cs ground state hyperfine splitting. For this a ratio like $f^{(\rm opt)}/f_{\rm Cs}^{(\rm HFS)}$ is determined. According to Table II such a ratio depends on two fundamental constants, α and the Cs nuclear magnetic moment measured in Bohr magneton's $\mu_{\rm Cs}/\mu_B$. One may argue that the latter is not a fundamental quantity, but one has to keep in mind that the nuclear moment is mostly determined by the strong interaction. In that sense it measures the strong interaction in some units. The only difference to the electromagnetic interaction measured by α is that, lacking a precise model for the Cs nucleus we are not sure what those units are. For this reason there are two parameters that need to be determined from an absolute optical frequency measurement and it is impossible to disentangle contribution from the drift rate of just one absolute optical frequency. As an example consider the frequency measurement of the $1S-2S$ transition in atomic hydrogen (see Fig. 15 (right) and Table I), for which the following expression for the relative drift rates derives [9]:

$$\begin{aligned} -\frac{\partial}{\partial t}\ln\frac{f_{\rm H}^{(\rm opt)}}{f_{\rm Cs}^{(\rm HFS)}} &= \frac{\partial}{\partial t}\left[\ln\left(\frac{\mu_{\rm Cs}}{\mu_B}\right) + (2+0.8)\ln\alpha\right] = \\ &= y + 2.8x = (3.2\pm 6.4)\times 10^{-15}\ \ \mathrm{yr}^{-1}\,, \end{aligned} \tag{21}$$

where the fractional time variations have been denoted by $y \equiv \partial \ln(\mu_{\rm Cs}/\mu_B)/\partial t$ and $x \equiv \partial \ln(\alpha)/\partial t$ respectively. From this relationship one can constrain a combination of the fractional time variation of $\mu_{\rm Cs}/\mu_B$ and α only. So far sufficiently precise hydrogen data has been obtained in 1999 and in 2003.

Between July 2000 and February 2006 the frequency of the electric quadrupole transition $5d^{10}6s\ ^2S_{1/2}\ (F=0) - 5d^9 6s^2\ ^2D_{5/2}\ (F'=2, m'_F=0)$ at $\lambda = 282\,\text{nm}$ of a single laser cooled $^{199}Hg^+$ ion was measured relative to a Cs-controlled hydrogen maser using the fs frequency comb technique [110]. These measurements have been performed in J. Bergquist's group at NIST resulting in a fractional frequency change of $(0.2\pm7.0)\times10^{-15}\ \text{yr}^{-1}$ if one considers only data taken during the period from July 2000 through December 2002 [111]. Including more recent measurements, the accuracy has been significantly improved such that for the whole period of measurements July 2000 to February 2006 the relative frequency ratio drift becomes experimentally limited to $\partial \ln(f_{\rm Hg}^{\rm (opt)}/f_{\rm Cs}^{\rm (HFS)})/\partial\, t = (0.37\pm0.39)\times10^{-15}\ \text{yr}^{-1}$. Rewriting this restriction in terms of x and y (see (21)) one gets

$$-\frac{\partial}{\partial t}\ln\frac{f_{\rm Hg}^{\rm (opt)}}{f_{\rm Cs}^{\rm (HFS)}} = \frac{\partial}{\partial t}\left[\ln\left(\frac{\mu_{\rm Cs}}{\mu_B}\right) + (2+0.8+3.2)\ln\alpha\right] = \\ = y + 6x = (-0.37\pm0.39)\times10^{-15}\ \ \text{yr}^{-1}. \tag{22}$$

At PTB, Braunschweig, Germany the frequency of the $6s\ ^2S_{1/2}(F=0) - 6s\ ^2D_{3/2}(F=3)$ electric quadrupole transition at $\lambda = 436\,\text{nm}$ of a single trapped and laser cooled $^{171}Yb^+$ ion was measured relative to a Cs controlled hydrogen maser using the fs frequency comb technique. The measurements that were performed by C. Tamm, E. Peik and co-workers between December 2000 and June 2006 resulted in a fractional frequency variation of $(0.78\pm1.40)\times10^{-15}$ per year [112, 113]:

$$-\frac{\partial}{\partial t}\ln\frac{f_{\rm Yb}^{\rm (opt)}}{f_{\rm Cs}^{\rm (HFS)}} = \frac{\partial}{\partial t}\left[\ln\left(\frac{\mu_{\rm Cs}}{\mu_B}\right) + (2+0.8-0.9)\ln\alpha\right] = \\ = y + 1.9x = (0.78\pm1.4)\times10^{-15}\ \ \text{yr}^{-1}. \tag{23}$$

In total the there are three independent laboratory drift measurements (21), (22) and (23) performed in overlapping time periods all of them consistent with zero drift. In order to use the hydrogen data, that enters now with the smallest weight, a linear drift scenario has to be assumed as the epochs only partially overlap.

Results of these measurements are shown in Fig. 19 (left), where the abscissa shows the sensitivity of the corresponding relativistic correction to a variation of α. Each of these measurement restricts the drift of a combination of different fundamental constants only. Of course it is desirable to disentangle individual contributions of the coupling constants. To solve this problem it may be assumed that only one coupling constant varies while other constants involved are fixed. However, within the framework of grand unification theories the strong, weak and electromagnetic coupling constants are expected to merge for higher energies. Therefore one expects that they can not vary independently. Assuming grand unification one can even derive a relation of the drift rates of hadron masses and nuclear g-factors that are determined by the strong interaction, and the relative drift rate of the fine structure constant: $\Delta m_p/m_p \approx \Delta g_{\rm nucl}/g_{\rm nucl} \approx \pm35\Delta\alpha/\alpha$ [13, 114]. The sign of the magnifying constant has to determined experimentally. Note that this relation may still be correct even if none of the constants are actually drifting.

Since there is neither an accepted model for violation of supersymmetric theory, neither a theory explaining the origin of fermion masses, all discussions about such correlations remain strongly model-dependent. For this reason one tries to avoid using any assumptions on correlations here. Fortunately, the dependence of the absolute optical frequencies in (21), (22) and (23) are linearly independent in the coupling constants, i.e. in x and y. To find a common solution including the corresponding uncertainties we assume that there are N independent experiments relating x and y to measured values b_i with uncertainties σ_i (one standard deviation) through:

$$y = A_i\, x + b_i \pm \sigma_i\,. \tag{24}$$

Here A_i are the coefficients which represent the sensitivity of the relativistic correction to the α variations (L_α). Let us assume Gaussian distribution of the data $P(x,y)$:

$$P(x,y) \propto e^{-\frac{1}{2}R^2(x,y)}\,, \quad \text{where} \quad R^2 = \sum_i \frac{1}{\sigma_i^2}(y - A_i\, x - b_i)^2\,. \tag{25}$$

The expectation values for the relative drift rates x and y are determined by the maximum likelihood method

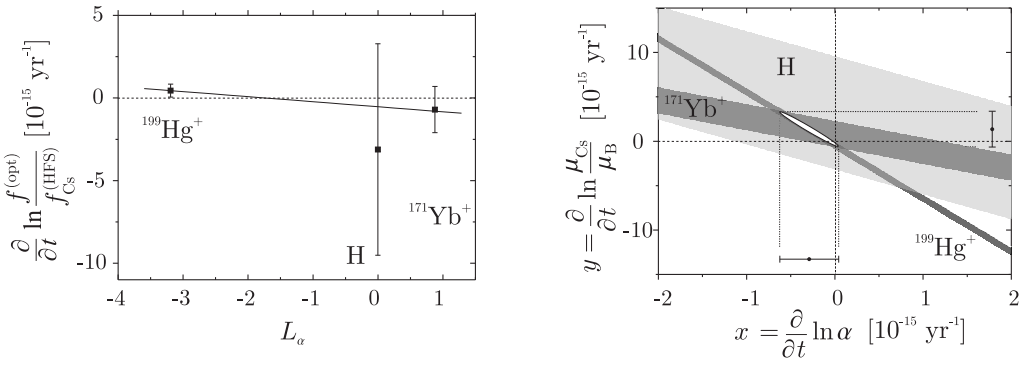

FIG. 19: *(left) — Measured drifts of optical frequencies for different atomic transitions vs. sensitivity of the relativistic correction to α variations. (right) — Model-independent constraints of fractional drift ratios of α and the Cs nuclear magnetic moment measured in Bohr magneton's μ_{Cs}/μ_B. The stripes represent experimental 1-σ restrictions deduced from different independent measurements. The ellipse defined by $R=1$ restricts the two-dimensional 1-σ area for the mean of x and y.*

corresponding to the minimum of $R^2(x,y)$:

$$\begin{aligned}\frac{\partial R^2}{\partial x} &= -2\sum\frac{1}{\sigma_i^2}(y-A_i\,x-b_i)A_i=0\\ \frac{\partial R^2}{\partial y} &= -2\sum\frac{1}{\sigma_i^2}(y-A_i\,x-b_i)=0\,.\end{aligned}\tag{26}$$

With the definitions $B_1\equiv\sum 1/\sigma_i^2$, $B_2\equiv\sum A_i^2/\sigma_i^2$, $B_3\equiv\sum b_i^2/\sigma_i^2$, $B_4\equiv\sum A_i/\sigma_i^2$, $B_5\equiv\sum b_i/\sigma_i^2$, $B_6\equiv\sum A_i\,b_i/\sigma_i^2$ we can solve system (26) for x and y and obtain expressions for the expectation values:

$$\langle x\rangle=\frac{B_4\,B_5-B_1\,B_6}{B_1\,B_2-B_4^2}\,,\qquad \langle y\rangle=\frac{B_2\,B_5-B_4\,B_6}{B_1\,B_2-B_4^2}\,.\tag{27}$$

The standard deviation for $\langle x\rangle$ can be calculated from the integral:

$$\int_{-\infty}^{+\infty}e^{-\frac{1}{2}R^2(x,y)}dy\propto\exp\left[\frac{(B_5+x\,B_4)^2-B_1(B_3+x\,(x\,B_2+2B_6))}{2B_1}\right]\,.\tag{28}$$

Rewriting the exponent

$$\exp\left[-\frac{(x-\langle x\rangle)^2}{2\sigma_x^2}+const_x\right]\,,\tag{29}$$

one gets the standard deviation for x

$$\sigma_x=\sqrt{\frac{B_1}{B_1\,B_2-B_4^2}}\tag{30}$$

and, similarly, for y

$$\sigma_y=\sqrt{\frac{B_2}{B_1\,B_2-B_4^2}}\,.\tag{31}$$

With this and the experimental data from (21), (22) and (23), stringent restrictions for fractional variations of the fundamental constants can be derived [110]:

$$x \;=\; \frac{\partial}{\partial t}\ln\alpha=(-0.30\pm0.35)\times10^{-15}\,\mathrm{yr}^{-1}\,,\tag{32}$$

$$y \;=\; \frac{\partial}{\partial t}\ln\frac{\mu_{\mathrm{Cs}}}{\mu_B}=(1.5\pm2.0)\times10^{-15}\,\mathrm{yr}^{-1}\,.\tag{33}$$

A graphical representation of the solution is shown in Fig. 19 (right). The ellipse defined by $R = 1$ restricts the 1σ area that is compatible with all observations. Projections of the ellipse on the axes give separate values for x and y as presented in (32) and (33) respectively. The result for the temporal variation of the fine structure constant now imposes a limit that is significantly smaller than drift rates derived from quasar absorption spectra [92, 93]. These astrophysical investigations correspond to the linear drift rate of $(\partial/\partial t) \ln \alpha = 0.64 \pm 0.14 \times 10^{-15}\,\mathrm{yr}^{-1}$ which is on the same level of sensitivity as the result of combined optical frequency measurements (32). However, as mentioned above, the two data sets are not strictly comparable as they probe on different epochs.

An extended time interval separating optical frequency measurements will improve the sensitivity of this laboratory test even further. Another promising route would be a direct comparison of two optical frequencies using the frequency comb without primary Cs reference [110]. In this case variations of the fine structure constant are probed independently because no nuclear magnetic moment enters.

VI. FURTHER PROSPECTS

The development of more stable and compact laser systems for the $1S-2S$ spectroscopy in atomic hydrogen opens an opportunity to perform spectroscopy on exotic simple atomic systems whose production or use is not possible at our Garching laboratories. This will require a new laser system to be set up close to the production and/or storage place. Together with a compact fiber-based frequency comb referenced to the GPS time signal, such a system will allow to perform absolute frequency measurements at any host laboratory. For example, experiments to study the $1S-2S$ spectroscopy in anti-hydrogen are prepared by the collaborations ATHENA (ALPHA) [115] and ATRAP [116] at CERN. A comparison between hydrogen and anti-hydrogen spectra should provide one of the most stringent tests of the CPT theorem. A frequency measurement of the $1S-2S$ transition in tritium could provide new independent information on the triton charge radius and its polarizability [117]. In addition, there are projects aiming for optical spectroscopy of positronium and muonium [118, 119].

The accuracy of the $1S-2S$ transition is presently limited by contributions of the spatially varying ac Stark shift and residual Doppler effects. To increase the accuracy and investigate other possible systematic shifts in more detail it is highly desirable to reduce the excitation power at 243 nm and select even slower atoms from the Maxwellian distribution. It has been shown [33], that along with excitation of the $1S-2S$ transition we can efficiently ionize the $2S$ state with the same laser beam. Since the detection efficiency for protons is much higher than for Lyman-α photons at nearly the same background count rate, one can detect signals from slower atoms or from atoms excited at lower excitation powers. We presently work on delayed proton detection, with the excitation cycle separated from ionization/detection cycle by hundreds of microsecond. Preliminary experiments show that this idea requires improved mechanical stability of the 243 nm enhancement cavity. We plan to use the idea of compensated suspension that has proofed to be a powerful method for the reference cavities [28].

Together with the expected new improved measurement of the proton charge radius derived from muonic hydrogen [84], further precision optical measurements in atomic hydrogen will deliver important experimental results for even more precise tests of QED and other fundamental theories.

VII. ACKNOWLEDGEMENTS

N.K. acknowledges the support of the Alexander von Humboldt Foundation, Russian Science Support Foundation and RFBR Grant #05-02-16801.

[1] John S. Ridgen, *Hydrogen: The Essential Element*, Harvard University Press, (2002).
[2] F. Biraben *et al.*, in: *The Hydrogen Atom. Precision Physics of Simple Atomic Systems*, edts. S.G. Karshenboim, F. S. Pavone, G. F. Bassani, M. Inguscio, T.W. Hänsch, Springer, Berlin, Heidelberg, 18 (2001)
[3] M. Weitz, A. Huber, F. Schmidt-Kaler, D. Leibfried, and T.W. Hänsch, Phys. Rev. Lett. **72**, 328 (1994)
[4] A. Huber, Th. Udem, B. Gross, J. Reichert, M. Kourogi, K. Pachucki, M. Weitz, and T.W. Hänsch, Phys. Rev. Lett., **80**, 468 (1998)
[5] N. Kolachevsky, M. Fischer, S.G. Karshenboim, T.W. Hänsch, Phys. Rev. Lett. **92**, 033003 (2004)
[6] N. Kolachevsky, P. Fendel, S.G. Karshenboim, T.W. Hänsch, Phys. Rev. A **70**, 063503 (2004)
[7] M.I. Eides, H. Grotch, and V.A. Shelyuto, Phys. Rep. **342**, 63 (2001)
[8] S.G. Karshenboim and V.G. Ivanov, Phys. Lett. B **524**, 259 (2002); Euro. Phys. J. D **19**, 13 (2002)
[9] M. Fischer *et al.*, Phys. Rev. Lett. **92**, 230802 (2004)

[10] R. Holzwarth *et al.*, Phys. Rev. Lett. **85**, 2264 (2000)
[11] Th. Udem, R. Holzwarth, T.W. Hänsch, Nature **416**, 233 (2002)
[12] L.S. Ma *et al.*, Science **303**(5665), 1843 (2004)
[13] X. Calmet, H. Fritzsch, Physics Letters B **540**, 173 (2002)
[14] T.R. Taylor and G. Veneziano, Phys. Lett. B **213**, 450 (1988)
[15] T. Damour, F. Piazza, G. Veneziano, Phys. Rev. Lett. **89**, 081601 (2002)
[16] V.V. Flambaum, E.V. Shuryak, physics/0701220
[17] V.V. Flambaum, arXiv:0705.3704v2 [physics.atom-ph]
[18] T.W. Hänsch, S.A. Lee, R. Wallenstein, and C. Wieman), Phys. Rev. Lett. **34**, 307 (1975)
[19] A. Huber, B. Gross, M. Weitz, and T. W. Hänsch Phys. Rev. A **59**, 1844 (1999)
[20] C.L. Cesar, D. Kleppner, Phys. Rev. A **59**, 4564 (1999)
[21] M. Haas *et al.*, Phys. Rev. A **73**, 052501 (2006)
[22] K.S.E. Eikema, J. Walz, and T.W. Hänsch, Phys. Rev. Lett. **86**, 5679 (2001)
[23] D. Kielpinski, Phys. Rev. A **73**, 063407 (2006)
[24] N. Kolachevsky, J. Alnis, S.D. Bergeson, and T.W. Hänsch, Phys. Rev. A **73**, 021801 (2006)
[25] H.R. Telle, in *Frequency Control of Semiconductor Lasers*, ed. M. Ohtsu, 137, Wiley, New York, (1996)
[26] R.W.P. Drever *et al.*, Appl. Phys. B **31**, 97 (1983)
[27] M. Fischer, N. Kolachevsky, M. Zimmermann *et al.* in: Lecture Notes in Physics: *Astrophysics, Clocks and Fundamental Constants*, edts. S.G. Karshenboim and E. Peik, Springer Verlag Berlin, Heidelberg, **648**, 209 (2004)
[28] A.D. Ludlow *et al.*, Optics Letters **32**, 641 (2007)
[29] M. Notcutt *et al.* Phys. Rev. A **73**, 031804R (2006)
[30] R. Lalezari, Advanced Thin Films, Longmont, CO
[31] L.-S. Ma, P. Jungner, J. Ye, and J. Hall, Opt. Lett. **19**, 1777 (1994)
[32] M. Okai, in *Frequency Control of Semiconductor Lasers*, ed. M. Ohtsu, 1, Wiley, New York, (1996)
[33] N. Kolachevsky *et al.*, Phys. Rev. A **74**, 052504 (2006)
[34] S.M. Rytov, Yu.A. Kravtsov, V.I. Tatarski, *Principles of statistical radiophysics 2*, p.59, Springer Verlag Berlin Heidelberg (1988)
[35] D.S. Elliot, M.W. Hamilton, K. Arnett, and S.J. Smith, Phys. Rev. Lett. **53**, 439 (1984)
[36] B.C. Young, F.C. Cruz, W.M. Itano, and J.C. Bergquist, Phys. Rev. Lett. **82**, 3799 (1999)
[37] K. Numata, A. Kemery, and J. Camp, Phys. Rev. Lett. **93**, 250602 (2004)
[38] G. Scoles, D. Bassi, U. Buck, and D. Laine, *Atomic and Molecular Beam Methods*, Band 1, Oxford University Press, New York (1988)
[39] L.O. Hocker,A. Javan, D.R. Rao, L. Frenkel, T. Sullivan, Appl. Phys. Lett. **10**, 147 (1967)
[40] K.M. Evenson, J.S. Wells, F.R. Petersen, B.L. Danielson, G.W. Day, Appl. Phys. Lett. **22**, 192 (1973)
[41] H. Schnatz, B. Lipphardt, J. Helmcke, F. Riehle, G. Zinner, Phys. Rev. Lett. **76**, 18 (1996)
[42] J.N. Eckstein, A.I. Ferguson, and T.W. Hänsch, Phys. Rev. Lett. **40**, 847 (1978)
[43] Th. Udem, J. Reichert, R. Holzwarth, T.W. Hänsch, Opt. Lett. **24**, 881 (1999)
[44] S.A. Diddams, L. Hollberg, L.S. Ma, L. Robertsson, Opt. Lett. **27**, 58 (2002)
[45] J. Reichert, R. Holzwarth, Th. Udem, T.W. Hänsch, Opt. Commun. **172**, 59 (1999)
[46] G.P. Agrawal, *Nonlinear Fiber Optics*, Academic Press, New York, (2001)
[47] S.A. Diddams *e al.*, Phys. Rev. Lett. **84**, 5102 (2000)
[48] J.C. Knight *et al.*, Opt. Lett. **21**, 1547 (1996)
[49] J.K. Ranka *et al.*, Opt. Lett. **25**, 25 (2000)
[50] P.St.J. Russell, Science **299**, 358 (2003)
[51] J. Reichert *et al.*, Phys. Rev. Lett. **84**, 3232 (2000)
[52] R. Holzwarth *et al.*, Laser Phys. **11**, 1100 (2001)
[53] R. Ell *et al.*, Opt. Lett. **26**, 373 (2001)
[54] T.M. Fortier *et al.*, Opt. Lett. **28**, 2198 (2003)
[55] L. Matos *et al.*, Opt. Lett. **29**, 1683 (2004)
[56] T.M. Fortier *et al.*, Opt. Lett. **31**, 1011 (2006)
[57] K.A. Corwn *et al.*, Phys. Rev. Lett. **90**, 113904 (2003)
[58] K.W. Holman *et al.*, Opt. Lett. **28**, 851 (2003)
[59] L.E. Nelson *et al.*, Appl. Phys. B **65**, 277 (1997)
[60] P. Kubina *et al.*, Opt. Express **13**, 909 (2005)
[61] F. Adler *et al.*, Opt. Express **12**, 5872 (2004)
[62] J.J. McFerran*et al.*, Opt. Lett. **31**, 1997 (2006)
[63] F.L. Walls and A. DeMarchi, IEEE Trans. Instrum. Meas. **24**, 210 (1975)
[64] Th. Udem *et al.*, Phys. Rev. Lett. **82**, 3568 (1999)
[65] H.A. Haus and E.P. Ippen, Opt. Lett. **26**, 1654 (2001)
[66] A. Hasegawa and F. Tappert, Appl. Phys. Lett. **23**, 142 (1973)
[67] L. Xu *et al.*, Opt. Lett. **21**, 2008 (1996)
[68] M. Prevedelli, T. Freegarde, and T.W. Hänsch, Appl. Phys. B **60**, S241 (1995)
[69] G. Santarelli *et al.*, Phys. Rev. Lett. **82**, 4619 (1999)
[70] M. Abgrall, Thèse de doctorat de l'université Paris VI (2003)

[71] M. Niering *et al.*, Phys. Rev. Lett. **84**, 5496 (2000)
[72] J.P. Mohr and B.N. Taylor, Physics Today **54**(3), 29 (2001)
[73] D.L. Farnham, R.S. Van Dyck, Jr., and P.B. Schwinberg, Phys. Rev. Lett. **75**, 3598 (1995)
[74] B. de Beauvoir B. *et al.*, Eur. Phys. Lett. D **12**, 61 (2000)
[75] E.W. Hagley, and F.M. Pipkin, Phys. Rev. Lett. **72**, 1172 (1994)
[76] D.J. Berkeland, E.A. Hinds, and M.G. Boshier, Phys. Rev. Lett. **75**, 2470 (1995)
[77] M. Weitz *et al.*, Phys. Rev. A **52**, 2664 (1995)
[78] S. Bourzeix *et al*, Phys. Rev. Lett. **76**, 384 (1996)
[79] J.P. Mohr and B.N. Taylor, Rev. Mod. Phys. **77**(3), 1 (2005)
[80] G.G. Simon, C. Schmitt, F. Borkovski, and V.H. Walter, Nucl. Phys. A **333**, 381 (1980)
[81] Krzysztof Pachucki, Phys. Rev. A **63**, 042503 (2001)
[82] G. Hagel, R. Battesti, F. Nez, L. Julien, and F. Biraben, Phys. Rev. Lett. **89**, 203001 (2002)
[83] P. Fendel, *Präzisionsspektroskopie an Wasserstoff und Deuterium*, Ph.D. thesis (in German), Ludwig-Maximilians University, Munich (2005)
[84] R. Pohl *et al.*, Hyperfine Interactions, **127**, 161 (2004)
[85] M. Herrmann *et al.*, *The* $1S-2S$ *transtion in singly ionized helium: Feasibility of high precision spectroscopy in the XUV* (to be published)
[86] J.W. Heberle, H.A. Reih, and P. Kusch, Phys. Rev. **101**, 612 (1956)
[87] H.A. Reich, J.W. Heberle, and P. Kusch, Phys. Rev. **104**, 1585 (1956)
[88] N.E. Rothery and E.A. Hessels, Phys. Rev. A **61**, 044501 (2000)
[89] P.A.M. Dirac, Nature (London) **139**, 323 (1937)
[90] J.P. Uzan, Rev. Mod. Phys. **75**, 403 (2003)
[91] Y. Fujii, *et al.*, Nucl. Phys. B, **573**, 377 (2000)
[92] J.K. Webb *et al.*, Phys. Rev. Lett **87**, 091301 (2001)
[93] M.T. Murphy, J.K. Webb, V.V. Flambaum, Mon. Not. Roy. Astron. Soc. **345**, 609 (2003)
[94] A. Ivanchik, A. Potekhin, and D. Varshalovich, Astron. and Astroph. **343**, 439 (1999)
[95] A. Ivanchik, P. Petitjean, E. Rodriguez, and D. Varshalovich, Astrophys. Space Sci. **283**, 583 (2003)
[96] H. Chand, R. Srianand, P. Petitjean, and B. Aracil, Astron. and Astroph. **417**, 853 (2004)
[97] R. Quast, D. Reimers, and S.A. Levshakov, Astron. and Astroph. **415**, 27 (2004)
[98] M.T Murphy *et al.*, arXiv:astro-ph/0612407 v1 and arXiv:astro-ph/0611080 v3
[99] Yasunori Fujii, Phys. Lett. B **573**, 39 (2003)
[100] M.P. Savedoff, Nature, **178**, 689 (1956)
[101] R. Minkowski and O.C. Wilson, Astrophys. J. **123**, 373 (1956)
[102] N.A. Demidov et al., in *Proceedings of the 6th European Frequency and Time Forum, Noordwijk, The Netherlands, 1992*, (European Space Agency, Noordwijk, 1992), 409 (1992)
[103] L.A. Breakiron, in *Proceedings of the 25th Annual Precise Time Interval Applications and Planning Meeting*, NASA Conference Publication No. 3267 [U.S. Naval Observatory Time Service Department (TSSI), Washington DC, 1993], 401
[104] J.D. Prestage, R.L. Tjoelker, and L. Maleki, *Phys. Rev. Lett.* **74**, 3511 (1995)
[105] H.B.G. Casimir, *On the Interaction Between Atomic Nuclei and Electrons*, Freeman, San Francisco, 54 (1963)
[106] V.A. Dzuba, V.V. Flambaum, and J.K. Webb, *Phys. Rev.* A **59**, 230 (1999); Phys. Rev. Lett. **82**, 888 (1999)
[107] H. Marion *et al.*, Phys. Rev. Lett. **90**, 150801, (2003)
[108] V.A. Dzuba and V.V. Flambaum, Phys. Rev. A **61**, 034502 (2000)
[109] A. Cingöz *et al.*, Phys. Rev. Lett. **98**, 040801 (2007)
[110] T.M. Fortier *et al.*, Phys. Rev. Lett. **98**, 070801 (2007)
[111] S. Bize *et al.*, Phys. Rev. Lett. **90**, 150802, (2003)
[112] E. Peik *et al.*, Phys. Rev. Lett. **93**, 170801 (2004)
[113] E. Peik *et al.*, arXiv:physics/0611088 (2006)
[114] X. Calmet, H. Fritzsch, Eur. Phys. J C **24**, 639 (2002)
[115] M. Amoretti *et al.*, Nature, **419**, 456 (2002)
[116] G. Gabrielse *et al.*, Phys. Rev. Lett. **89**, 213401 (2002)
[117] B.F. Gibson, Lect. Notes in Phys. **260**, 511 (1986)
[118] R. Ley, Applied Surface Science, **194**, 301 (2002)
[119] K. Jungmann *et al.*, Z. Phys. D **21**, 241 (1991)
[120] some authors refer to these fibers as photonic crystal fibers that need to be distinguished form photonic bandgap fibers. The latter use Bragg diffraction to guide the light, while the fibers discussed here use the traditional index step, with the refractive index determined by the air filling factor.